

# The HST/ACS Coma Cluster Survey XI - The Luminosity Function of Galaxies in the Coma Cluster

N. Trentham<sup>1</sup>, B. Mobasher<sup>2</sup>, H. C. Ferguson<sup>3</sup>, D. Carter<sup>4</sup>, R. B. Tully<sup>5</sup>, M. Balcells<sup>6</sup>, T. J. Bridges<sup>7</sup>, K. Chiboucas<sup>5,8</sup>, P. Goudfrooij<sup>3</sup>, Alister W. Graham<sup>9</sup>, R. Guzmán<sup>10</sup>, D. Hammer<sup>3,11,12</sup>, A. Hornschemeier<sup>11,12</sup>, C. Hoyos<sup>10,13</sup>, A. Huxor<sup>14</sup>, S. Jogee<sup>15</sup>, R. Marzke<sup>16</sup>, E. W. Peng<sup>17,18</sup>, S. Phillipps<sup>14</sup>, J. Price<sup>14</sup>, T. Weinzirl<sup>15</sup>

<sup>1</sup>*Institute of Astronomy, Madingley Road, Cambridge, CB4 3IB, UK*

<sup>2</sup>*Department of Physics and Astronomy, University of California, Riverside, 900 University Avenue, Riverside, CA 92521, USA*

<sup>3</sup>*Space Telescope Science Institute, 3700 San Martin Drive, Baltimore, MD 21218, USA*

<sup>4</sup>*Astrophysics Research Institute, Liverpool John Moores University, IC2 Liverpool Science Park, 146 Brownlow Hill, Liverpool, L3 5RF, UK*

<sup>5</sup>*Institute for Astronomy, University of Hawaii, 2680 Woodlawn Drive, Honolulu, HI 96822, USA*

<sup>6</sup>*Instituto de Astrofísica de Canarias, C/Vía Lactea s/n, 38200 La Laguna, Tenerife, Spain*

<sup>7</sup>*Department of Physics, Engineering Physics, and Astronomy, Queen's University, Kingston, Ontario, K7L 5N6, Canada*

<sup>8</sup>*Gemini Observatory, 670 North A'ohoku Place, Hilo HI 96720, USA*

<sup>9</sup>*Centre for Astrophysics and Supercomputing, Swinburne University of Technology, Hawthorne, VIC 3122, Australia*

<sup>10</sup>*Department of Astronomy, University of Florida, 211 Bryant Space Science Center, Gainesville, FL 32611-2055, USA*

<sup>11</sup>*Department of Physics and Astronomy, Johns Hopkins University, 3400 North Charles Street, Baltimore MD 21218, USA*

<sup>12</sup>*Laboratory for X-ray Astrophysics, NASA GSFC Code 662.0*

<sup>13</sup>*Departamento de Física Teórica, Uni. Autónoma de Madrid, Carretera de Colmenar Viejo Km 15.600 Cantoblanco 28049 Madrid, Spain*

<sup>14</sup>*Astrophysics Group, H.H. Wills Physics Laboratory, University of Bristol, Tyndall Avenue, Bristol BS8 1TL, UK*

<sup>15</sup>*Department of Astronomy, 2515 Speedway, Stop C1400 Austin TX 78712-1205*

<sup>16</sup>*Department of Physics and Astronomy, San Francisco State University, San Francisco, CA 94132, USA*

<sup>17</sup>*Department of Astronomy, Peking University, Beijing 100871, China*

<sup>18</sup>*Kavli Institute for Astronomy and Astrophysics, Peking University, Beijing 100871, China*

9 December 2014

## ABSTRACT

We present the luminosity function of the Coma Cluster down to absolute  $I$  magnitude  $M_I = -11$  mag ( $M_V \approx -10$  mag,  $M_B \approx -9$  mag) from the HST/ACS Coma Cluster Survey. The ACS data were used to create a large sample of galaxies for spectroscopy at intermediate magnitudes and to make detailed morphological assessments of galaxies at faint magnitudes. There are 467 candidate members in the sample. Brighter than  $M_I = -17$  mag the luminosity function agrees with previous determinations. Between  $M_I = -17$  mag and  $M_I = -13$  mag, the luminosity function is rising with average logarithmic slope  $\alpha = -1.5$ . Between  $M_I = -13$  mag and  $M_I = -11$  mag, the luminosity function is flat or gradually falling with  $\alpha = -0.9$ . Fainter than  $M_I = -11$  mag we cannot measure the luminosity function because we cannot distinguish cluster galaxies from background galaxies with any confidence, even with the resolution of the ACS data. Most of the low-luminosity galaxies are dwarf elliptical galaxies.

**Key words:** galaxies: photometry – galaxies: clusters: individual: Coma Cluster – galaxies: luminosity function – galaxies: mass function

## 1 INTRODUCTION

Galaxies are frequently found in groups and clusters. In the largest clusters, most luminous galaxies are giant ellipticals and lenticulars while most low-luminosity galaxies are dwarf ellipticals. These clusters also contain considerable amounts

of hot x-ray gas in rough thermal equilibrium with the galaxies and cluster dark matter. The approximate ratio of dark matter, x-ray gas and stars in galaxies is 40:7:1 by mass in galaxy clusters, close to the cosmic ratio (Fukugita & Peebles 2004).

At a distance of 100 Mpc (redshift  $z = 0.023$ ), the

Coma Cluster is the best-studied rich cluster. It has a galaxy density several times that of the Virgo Cluster, the largest structure in the Local Supercluster. The Coma Cluster is unusual in that it is dominated by two luminous elliptical galaxies, NGC 4874 and NGC 4889, unlike many other rich clusters which have a single brightest cluster member or cD galaxy at their core (however see Postman & Lauer 1995). The Coma Cluster is also very luminous in x-rays, centered close to NGC 4874 (Chanan & Abramapolous 1984), which also has an extended stellar halo (Hoessel & Schneider 1985), characteristic of brightest cluster members and cD galaxies (Schombert 1988). There is a large group of galaxies infalling into the southwest of the Coma Cluster, centered on NGC 4839, the third-ranked cluster galaxy (Neumann et al. 2001, Adami et al. 2005).

Because of the proximity of the Coma Cluster, it has become a benchmark for comparison with galaxy properties in other clusters and theory. The luminosity function (LF)  $\phi(L)$  of galaxies is widely used in exploring the statistical properties of galaxies. It is defined such that  $\phi(L)dL$  is the number density of galaxies with luminosities between  $L$  and  $L + dL$ . At a general level, the LF is described in most environments by a Schechter (1976) function consisting of an exponential drop-off at high, and a power-law rise at low, luminosities. The logarithmic slope at low luminosities  $\alpha$  provides a measure of the number of very small galaxies (if  $\alpha = -1$ , the LF is flat and there are roughly the same number of large and small galaxies but if  $\alpha = -2$ , the LF is steep and there are many more small and faint galaxies). For comparison, the dark matter halo mass function predicted from  $\Lambda$ CDM theory has a slope  $\alpha \sim -2$  at low masses. The luminosity function is often presented as a magnitude function  $\phi(M) = -\phi(L) \frac{dL}{dM}$  which has faint-end slope  $-0.4(1 + \alpha)$ .

The shape of the LF is constrained by a number of different physical processes and the complex interplay between them, including:

- (i) the gravitational growth of dark matter perturbations, described by the power spectrum;
- (ii) the infall of gas from the intergalactic medium into dark matter condensations;
- (iii) the retention of this gas by dark matter halos, as the gas is heated up by the metagalactic UV flux;
- (iv) the conversion of gas into stars;
- (v) mergers of galaxies and cannibalism of smaller galaxies by larger systems.

The relative importance of these processes is a strong function of environment. For example, in most of the environments studied to date, the LF is much shallower than that predicted from the dark-matter halo mass function, suggesting that the cumulative effect of (iii)+(iv) suppresses star formation activity preferentially in smaller galaxies (this is the cosmic missing satellite problem; Moore et al. 1999, Klypin et al. 1999). Moreover, the LF appears to be flatter in the field than in clusters (Trentham, Sampson & Banerji 2005 and references therein), which could result from a variety of mechanisms. For example, small galaxies are likely to perform (ii) more efficiently if they assemble early, and galaxies which assemble early in the history of the Universe are the ones which end up in clusters (Tully et al. 2002). Furthermore, increased tidal activity during cluster assembly probably results in (iv) being more efficient for galaxies

in clusters. This environmental dependence of the LF has been investigated theoretically using the conditional luminosity function (Cooray 2006, Yang, Mo & van den Bosch 2008) which describes the LF as a function of parent halo mass.

Early studies of the Coma cluster LF (e.g. Godwin & Peach 1977, Thompson & Gregory 1993) concentrated on the magnitude regime  $I < 19$  mag (absolute magnitudes  $M_I < -16$  mag, equivalently  $M_B < -14$  mag in the  $B$ -band), where the cluster is seen as an obvious contrast against the background. At fainter magnitudes, background contamination becomes a serious problem because the Coma Cluster is sufficiently distant that member galaxies cannot be easily distinguished from background galaxies along the Coma Cluster line of sight (Gutierrez et al. 2004). However, they can be identified as cluster members if they have extremely low surface brightnesses (Karachentsev et al. 1995, Adami et al. 2006). Further complications result from the large field-to-field variance of the background galaxy counts due to more distant large-scale structure which means that a straightforward background subtraction (Driver et al. 1998) will result in very substantial uncertainties at faint magnitudes. This significantly limits measurement of the faint-end of the LFs from recent studies (Bernstein et al. 1995, Biviano et al. 1995, Secker 1996, Secker & Harris 1996, Lobo et al. 1997, Trentham 1997, Adami et al. 2000, Beijersbergen et al. 2002, Andreon & Cuillandre 2002, Adami et al. 2007a, Adami et al. 2007b, Milne et al. 2007, Michard & Andreon 2008, Yamanoi et al. 2012). While colour information (e.g. Adami et al. 2008) may help, the uncertainties are still large. The most secure technique for measuring the LF is using spectroscopic redshifts. Spectroscopic measurements of the LF have been performed down to  $M_R = -13$  mag (Mobasher et al. 2003), approximately  $M_B = -12$  mag.

In this paper, we use a deep imaging survey of the Coma cluster, obtained using Advanced Camera for Survey on board the Hubble Space Telescope (Carter et al. 2008) to establish the LF of the Coma Cluster two magnitudes deeper than previous studies. The ACS images are used for two purposes:

- 1) the images are used to select galaxies for spectroscopic follow-up, and
- 2) the high-resolution images are used to obtain detailed morphological information about the galaxies so as to extend the LF of the Coma cluster to fainter limits ( $M_I = -11$  mag). Fainter than this, our inability to distinguish members from background galaxies limits the measurement of the LF. We can *detect* galaxies with  $M_I > -11$  mag, but we cannot determine how likely they are to be cluster members.

The paper is structured as follows. In Section 2 we describe our observations, followed by the compilation and selection of our sample in Section 3. Measurement of the LF is presented in Section 4. In Section 5 we discuss the results and place them in the wider context of galaxy formation. Our conclusions are summarized in Section 6. Throughout this paper we assume a distance modulus to the Coma Cluster of 35.0 mag, corresponding to a distance of 100 Mpc.

## 2 OBSERVATIONS

### 2.1 The Imaging Survey

The *HST*/ACS observations used in this program are described in Carter et al. (2008). In summary, we observed 21 pointings (each 11 arcmin<sup>2</sup>) around the centre of the Coma cluster. The duration for each pointing was one orbit for each filter F475W (approximately Gunn *g*) and F814W (approximately Cousins *I*). The combination of these filters provide high resolution colours for each galaxy. The locations of each of the fields is presented in Figure 1 and Table 1. Using the SExtractor program (Bertin and Arnouts 1996), we generated a galaxy catalogue (Hammer et al. 2010). There are about 10<sup>5</sup> objects listed in the catalog.

### 2.2 Spectroscopic observations

#### 2.2.1 Hectospec observations

In Spring 2008 and Spring 2009, the spectroscopic survey was carried out over 6000 galaxies using the Hectospec spectrograph on the MMT 6 m telescope (Fabricant et al. 2005). Many of these were in the region surveyed by ACS. The survey is described in detail by Marzke et al. (in preparation).

Targets were selected from SDSS imaging based on their apparent magnitude,  $g - r$  colour and surface brightness. In the regions observed with HST/ACS, the overall spectroscopic completeness is 90% at  $r = 19.9$  mag and 50% at  $r = 20.8$  mag. A 270 lines/mm grating was used, which gives approximately 4.5 Å resolution at a pixel scale of 1.21 Å/pixel. In most cases, the total integration time was one hour and the useful spectral range is approximately 3700–9000 Å. The seeing was 0.7'' to 1.8'', comparable to the 1.5'' fibre diameter, corresponding to 730 pc at the distance of the Coma Cluster.

The data were reduced and redshifts determined using both HSRED (written by Richard Cool which determines redshifts using a  $\chi^2$  minimization) and XCSAO (Kurtz & Mink 1998 which determines redshifts by correlating spectra with SDSS templates). Finally, the quality of each spectrum was judged by eye and a list of redshifts compiled.

Finally, the spectra were cross-referenced with the ACS sample. The intention was to get a reasonably complete list of members in the ACS fields with  $I < 19$  mag as well as to identify galaxies with  $19 \text{ mag} < I < 21$  mag which are members but were compact enough to look like background galaxies in the imaging data.

#### 2.2.2 LRIS observations

The motivation for the Keck LRIS spectroscopic observations was very different from that of the Hectospec observations. Here the intention was to study a small number of typical faint ( $20 \text{ mag} < I < 23 \text{ mag}$ ) low surface-brightness (LSB) galaxies in order to examine our membership assessments based on morphology in the ACS images. Only then can we have confidence in the LF constructed this way. The instrumental configuration reflected this need and is described in detail in Chiboucas et al. (2010).

Observations were made with the LRIS multi-object spectrograph on the Keck 10 m Telescope over two nights, 2-3 April 2008. We observed 4 masks for 3.5 hours each,

**Table 1.** The ACS fields

Visit	$\alpha$ (J2000)	$\delta$ (J2000)
1	195.1956	28.0819
2	195.1307	28.0817
3	195.0662	28.0817
8	195.1805	28.0286
9	195.1156	28.0286
10	195.0508	28.0288
12	194.9208	28.0284
13	194.8559	28.0282
14	194.7904	28.0284
15	195.1651	27.9754
16	195.1003	27.9754
18	194.9702	27.9754
19	194.9056	27.9756
22	195.1504	27.9222
23	195.0854	27.9222
24	195.0204	27.9222
25	194.9554	27.9222
33	194.8753	27.8964
45	194.5930	27.4589
46	194.6458	27.3828
59	194.6344	27.2001
63	194.1283	27.2268
75	194.7031	27.7700
78	194.2983	27.4025
90	194.2716	27.5250

with  $\sim 35$  targets per mask. In total, we observed 73 possible members (rated 1-3 according to the prescription in the next section) and 20 expected background galaxies. A further 47 ultracompact dwarf (UCD) candidates were also observed with the same masks.

The spectroscopic setup reflected the need to maximize S/N at the expense of the resolution. The spectral range was chosen to include the Ca H and K lines and the Balmer break at the blue end. Using the 5600 Å dichroic to split the light between blue and red chips, we reached the Ca triplet on the red side. For these low-surface brightness galaxies, the blue-side absorption features were more critical for redshift measurements. The red-side data were used primarily for detecting background galaxy emission lines. For the blue spectra, a 400 line mm<sup>-1</sup> grism blazed at 3400 Å provided a 1.07 Å pix<sup>-1</sup> dispersion, peak efficiency of 75% at 3900 Å, and a resolution of 7.8 Å FWHM with 1.2 arcsec slitlets. On the red side, we used the 400 line mm<sup>-1</sup> grating blazed at 8500 Å providing 1.92 Å pix<sup>-1</sup> dispersion. Total integrations for each of 4 masks were 8 × 1500 s. Calibration arc lamps were observed each night and sky lines were used to correct for shifts in the observations. However, the prominent 5577 Å line fell on the edge of our spectra or, depending on the location on the mask, off the observed spectra altogether. Due to uncertainties in the applied shift, we therefore expect systematic errors of up to 100 km s<sup>-1</sup> in our radial velocity measurements.

Data were processed using the standard procedures in IRAF to bias correct, flatten, rectify, wavelength calibrate, and extract 1-D spectra. Redshifts were extracted from the

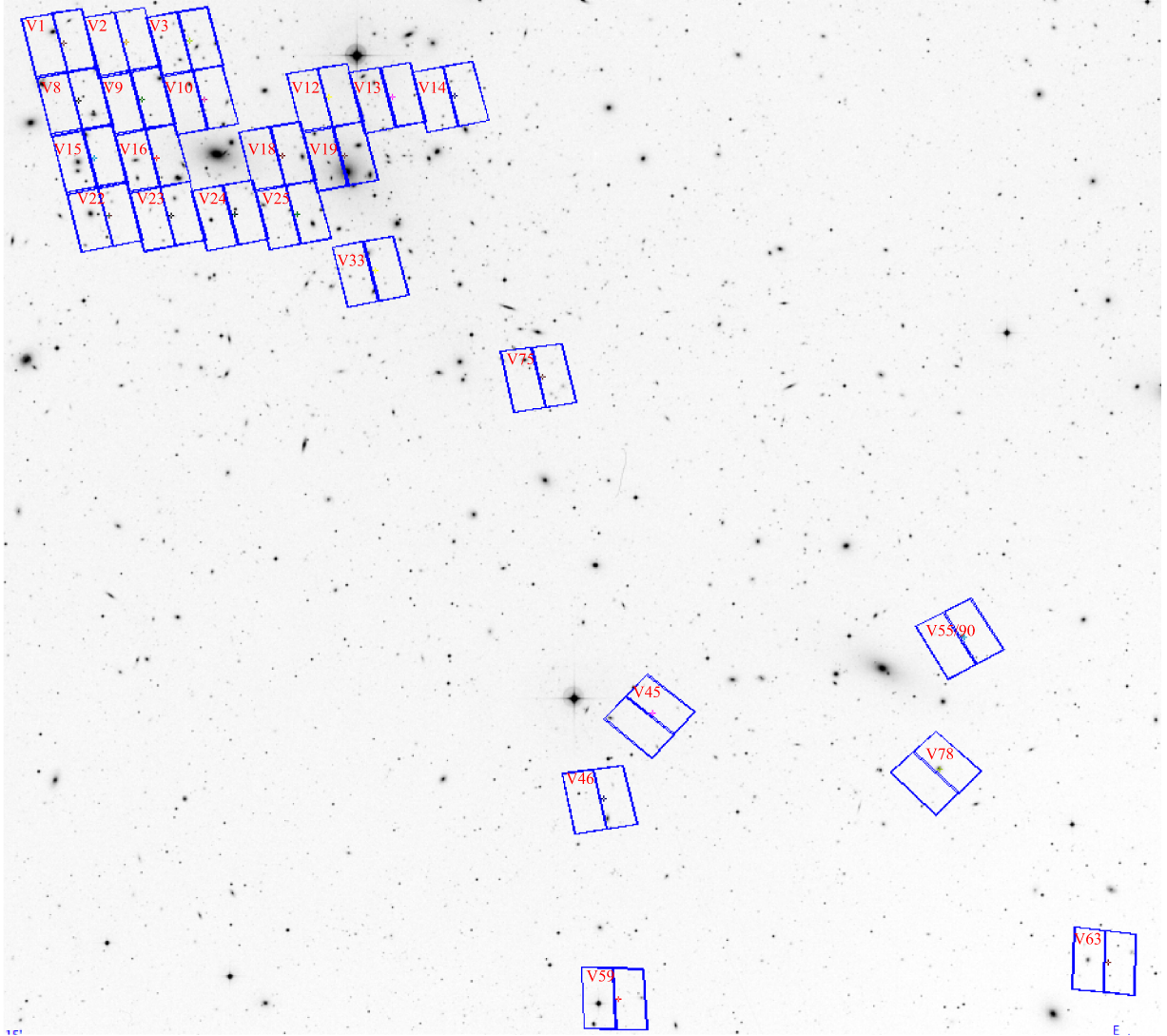


**Figure 1.** The ACS fields superimposed on the Digital Sky Survey. The image is  $1.5^\circ \times 1.5^\circ$ . North is up and east is to the left

final spectra, using the RVSAO/XCSAO package from cross-correlation with absorption and emission line template spectra. Of the 93 galaxies targeted, we successfully measured redshifts for 50 members and 20 background galaxies. Another 8 spectra with low S/N ( $< 3$ ) or with single emission lines provided uncertain measurements for 2 possible members and 6 possible background galaxies. For 15 spectra, the S/N was too low to measure redshifts, including 12 likely members and 3 expected background galaxies.

### 3 CLUSTER MEMBERSHIP AND THE CATALOG

In the local Universe, almost all dwarf galaxies are low-surface-brightness galaxies (exceptions like M32 and other compact ellipticals are rare). The *HST* resolution is sufficient to distinguish low-surface-brightness galaxies from faint stars and compact galaxies brighter than  $m_{F814W} = 24$  mag. Within the area of the ACS data, there are several thousand galaxies listed in the SExtractor catalog (Hammer et al. 2010) with  $m_{F814} < 24$  mag. This is typical for blank regions of sky; given the compilation of Metcalfe et al. 2001, we would expect about 5600 field galaxies with  $I < 24$  mag

**Table 2.** Number of Galaxies with Spectroscopic Confirmation

$m_{F814W}$	$N_{\text{total}}$	$N_{\text{cand,mem}}$	$N_{\text{v,mem}}$	$N_{\text{v,bkg}}$
< 16.0	44	44	44	0
16.0 – 16.5	8	7	7	1
16.5 – 17.0	12	12	12	0
17.0 – 17.5	14	13	13	1
17.5 – 18.0	14	10	9	4
18.0 – 18.5	30	19	13	8
18.5 – 19.0	34	13	10	15
19.0 – 19.5	57	18	14	26
19.5 – 20.0	82	17	12	37
20.0 – 20.5	132	25	13	46
20.5 – 21.0	186	31	12	38
21.0 – 21.5	296	29	10	25
21.5 – 22.0	466	34	10	15
22.0 – 22.5	614	48	7	3
22.5 – 23.0	926	56	3	3
23.0 – 23.5	1450	50	0	5
23.5 – 24.0	2305	41	0	6

in the survey area. Brighter than  $m_{F814W} = 24$  mag there are only a few hundred low-surface brightness galaxies in the survey area, suggesting that  $> 90\%$  of the galaxies are background objects or cluster globular clusters (Peng et al. 2009). In Table 2 we list, as a function of apparent magnitude, the total number of galaxies in the SExtractor catalog ( $N_{\text{tot}}$ ), the number of candidate (as defined later in this section) members ( $N_{\text{cand,mem}}$ ), the number of members with a velocity measurement ( $N_{\text{v,mem}}$ ), and the number of galaxies with a velocity measurement that puts it in the background ( $N_{\text{v,bkg}}$ ).

The majority of these low-surface brightness galaxies were detected and listed in the SExtractor catalog. They could be identified in a magnitude-surface brightness diagram constructed from the catalog. However the most extreme objects were not detected or were deblended into several smaller sources. Therefore we use a listing obtained from visual inspection in order to construct a galaxy sample for the LF. Here we use the F814W data to determine the LF in the  $I$ -band. This is deeper than the data taken in the bluer (F475W) filter.

In order to unambiguously establish membership, spectroscopic velocities are required. Velocities are easiest to obtain for more luminous and higher surface-brightness galaxies. Table 2 shows how many galaxies have velocities as a function of apparent magnitude. Following Colless & Dunn (1996) we assume that a galaxy is a member of the Coma cluster if its heliocentric velocity is between  $4000 \text{ km s}^{-1}$  and  $10000 \text{ km s}^{-1}$ .

For faint galaxies and those with low surface brightnesses, it is not possible to obtain spectra because they require long integration times, even with the largest telescopes. For these galaxies, we need some other criteria to establish membership. In general, lower surface brightness galaxies of a given apparent magnitude have a higher probability of being a member because dwarf galaxies have intrinsically low surface brightness and surface brightness is not

a function of distance. The advantage of the current data over previous data is that the angular resolution is so high, permitting us to make assessments down to very faint levels, where the galaxies are small. However, surface brightness is only one of many factors that need to be considered when establishing the membership probability. Detailed knowledge of morphology is necessary as well. If a galaxy exhibits weak evidence of spiral structure (here we mean spiral structure in a low-surface brightness galaxy that we cannot assert is real at a high level of confidence due to the low signal-to-noise, not weak spiral structure in an otherwise smooth galaxy; Graham et al. 2003), or has a chain morphology, we expect it to lie in the background even if the surface brightness is low. This assessment is primarily subjective; quantities like Gini and  $m20$  (Lisker 2008) are of limited use because they are dominated by the contribution from light near the centre of the galaxy, which is not the light used to make the morphology assessment.

Galaxies with extremely low surface brightness that are not accessible to spectroscopy have very few field counterparts, so they are probably cluster members. The intermediate range, where the surface brightness is low enough that a galaxy is a likely member yet high enough that we cannot assert this with a high degree of confidence is small so our sample is not dominated by these marginal cases except at faint magnitudes. Spectrographs like LRIS are sufficiently sensitive that spectra can be obtained and velocities determined for galaxies as faint as  $I = 23$  mag. At the very faintest magnitudes ( $I > 24$  mag), galaxies are too small to allow distinction between background and cluster members with any confidence, even with the ACS images.

The problem is that the information that is most important in any particular case is located at different places in each galaxy and is often subtle and only depends on the morphology and structure of a small fraction of the total light. Therefore it is not straightforward to construct a framework in which the probabilities depend on some combination of structural parameters. Rather, we rely on subjective assessments based on our knowledge of the morphologies of galaxies. Colour information would be of limited value since most contaminants are in the near background and would have similar colours to cluster members. We checked our sample for anomalously red  $m_{F475W} - m_{F814W}$  colours; this would have revealed any very distant groups of galaxies, which looked like a single nearby dwarf galaxy because of cosmological surface brightness dimming.

Having identified candidate members, each was examined visually and was given a rating 0 to 4, defined as:

0 – membership confirmed by velocity. These galaxies have a heliocentric velocity in the range  $4000 \text{ km s}^{-1} < V_h < 10000 \text{ km s}^{-1}$ .

1 – galaxies that are almost certain to be members, as they do not exist in significant numbers in the field. These are mostly the very low surface brightness (VLSB) galaxies. Often these were not detected in the automated catalog.

2 – galaxies that are likely members, but with a lower membership probability than those rated 1.

3 – galaxies that have an appreciable probability of being members but also an appreciable probability of lying in the background. That there is a significant number of galaxies

with this rating follows from the existence of large scale structure in the near-background (Adami et al. 2009)

4 – galaxies that will most certainly lie in the background. Mostly this is because they are compact, but occasionally it is because they have morphological features like spiral structure, indicating the galaxy is probably luminous and hence in the background. This category represents the vast majority of the galaxies at faint magnitudes.

On the occasions when we determined ratings for galaxies where spectroscopic redshifts subsequently became available, galaxies rated 1 or 2 were found to be members  $>90\%$  of the time and galaxies rated 3 were found to be members about 50% of the time. These percentages come from the *LRIS* observations described in Section 2.3 (Chiboucas et al. 2010) which included galaxies as faint as  $m_{F814W} = 22.8$  mag. Less than 1% of galaxies rated 4 turned out to be members (these were always compact ellipticals; Price et al. 2009). Such galaxies are rare and comprise about 1% of the cluster galaxy population. Here the percentages come from the Hectospec observations described in Section 2.2 (large numbers of velocities were obtained for galaxies with  $m_{F814W} < 20$  mag) as well as the *LRIS* observations described in Section 2.3 (small numbers of velocities were obtained for the fainter galaxies rated 4).

The total magnitude for each galaxy was estimated from its isophotal (for compact and bright galaxies) and aperture (for faint galaxies) magnitudes. In general, the light profile for the LSB cluster members is noisy with low  $S/N$ . For these systems, the total magnitude was estimated using the aperture magnitude at the radius at which the galaxy has comparable  $S/N$  to the sky. Uncertainties were typically 0.2 mag (they were larger for the lowest surface-brightness galaxies because such a large fraction of the counts were due to the sky). For these sources, the total magnitudes were often significantly different from those in the source catalog, probably because most members are LSB galaxies with unusual sizes and shapes. A comparison between these total magnitudes and candidate magnitudes is presented in Figure 2. The agreement is normally very poor for the lowest surface brightness galaxies (typically rated 1) but good for compact and bright galaxies (rated 0). Galaxy types were determined from the profile decompositions of Weinzirl et al. (2014) for the bright galaxies and by visual inspection for the faint galaxies. A designation dE/I means that the we were unable to distinguish between dwarf elliptical and dwarf irregular galaxies from the images.

The sample contains 467 member galaxies in classes 0–3. These galaxies are listed in Table 3. The brighter galaxies in Table 3 have various names, including those given by Rood & Baum (1967; designated RB) and the Sloan Digital Sky Survey (SDSS). The compact galaxies with CcGV designations are from Price et al. (2009). Many of the sources have GMP83 designations (Godwin, Metcalfe & Peach 1983) but we do not give those individually. The faintest galaxies in the table have  $I = 24$  mag, about two magnitudes brighter than our point source limiting magnitude (Carter et al. 2008). This is because at  $m_{F814W} > 24$  mag we cannot distinguish members from background galaxies.

This strategy selects against compact stellar systems including UCDs which appear to be common in the Coma Cluster at faint magnitudes (although less common than normal low-surface brightness dwarf galaxies). However it is

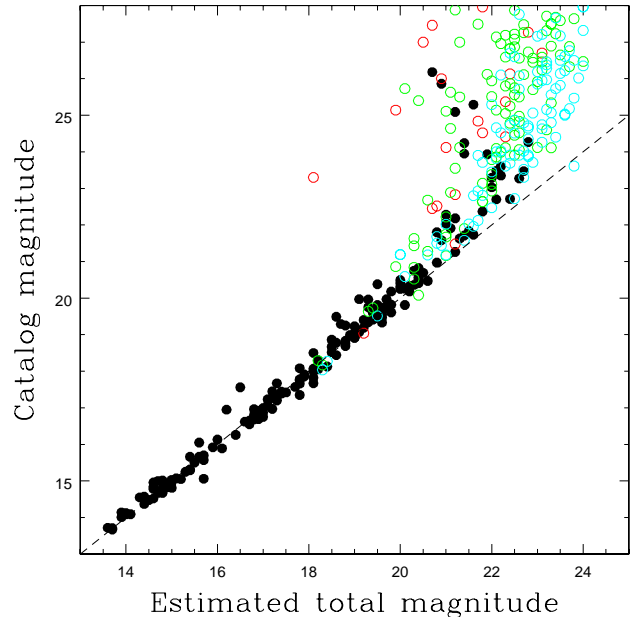


**Figure 2.** The estimated total magnitude (computed as described in the text) compared with the SExtractor auto magnitude for the candidate galaxies. The colours are for galaxies with the following ratings: black – rating 0, red – rating 1, green – rating 2, cyan – rating 3.

still unclear whether these should be considered as an independent class of galaxy, each with their own dark-matter halo, in which case they should be included in the luminosity function. Nevertheless, the results of this paper are complementary to those studying the properties of the UCDs and both will need to be taken into account when reconstructing the history of the Coma Cluster.

Comments on individual objects:

**Object 29:** contains an unusual feature in the shape of a cross below the central regions of the galaxy.

**Object 48:** could be either a background galaxy or a member with very high velocity.

**Object 115:** this object has an enormous LSB plume to the west.

**Object 127:** compact object in IC 4045 halo.

**Object 149:** VLSB object that is part of the larger feature discussed by Trentham & Mobasher (1998).

**Object 155:** extremely compact galaxy

**Object 156:** well inside the NGC 4874 halo.

**Object 224:** contains an unusual elongated nucleus.

#### 4 THE LUMINOSITY FUNCTION

The F814W filter is similar to the  $I$ -band filter (ACS Instrument Handbook) so we use  $m_{F814W}$  as an approximation to the  $I$ -band apparent magnitude  $m_I$ . In this work, luminosity functions are presented for the  $I$  band. Magnitudes can be converted to other filters using galaxy colours tabulated by Fukugita, Shimasaku & Ikeuchi (1995) and LFs for those filters can be constructed. The absolute magnitude for each galaxy  $M_I$ , is determined from the relation

**Table 3.** Members and Candidate Members of the Coma Cluster

ID	Name	Rating	Type	Visit	$V_h$ (km s <sup>-1</sup> )	$\alpha$ (J2000)	$\delta$ (J2000)	$m_{F814}$
1	NGC 4874	0	E	19	7165	194.8988	27.9593	12.1
2	IC 4045	0	E	1	6895	195.2026	28.0906	13.6
3	IC 4051	0	E	8	8724	195.2148	28.0429	13.7
4	IC 4042	0	S0	15	6356	195.1782	27.9713	13.7
5	NGC 4898a	0	pec	16	6895	195.0737	27.9553	13.7
6	NGC 4871	0	S0	19	6775	194.8749	27.9564	13.9
7	IC 3973	0	Sa	33	4707	194.8784	27.8842	13.9
8	NGC 4873	0	E	19	5816	194.8866	27.9836	14.0
9	NGC 4906	0	E	22	7495	195.1657	27.9240	14.0
10	IC 3976	0	E	33	6805	194.8725	27.8501	14.0
11	NGC 4876	0	E	25	6715	194.9350	27.9125	14.1
12	IC 4026	0	S0	9	8154	195.0922	28.0470	14.3
13	IC 4041	0	S0	15	7075	195.1702	27.9966	14.4
14	IC 3998	0	S0	18	9383	194.9449	27.9739	14.4
15	IC 3947	0	E	75	5666	194.7171	27.7851	14.4
16	RB 026	0	S0	13	6895	194.8810	28.0466	14.5
17	IC 4040	0	Scd	8	7855	195.1581	28.0574	14.6
18	RB 110	0	E	8	7615	195.1615	28.0145	14.6
19	IC 4021	0	E	10	5726	195.0614	28.0413	14.6
20	IC 4042A	0	S0/a	15	8394	195.1785	27.9631	14.6
21	NGC 4898b	0	pec	16	6356	195.0754	27.9566	14.7
22	RB 087	0	S0	3	7495	195.0536	28.0755	14.8
23	IC 4033	0	S0	16	7705	195.1183	27.9724	14.8
24	NGC 4894	0	S0	16	4617	195.0688	27.9675	14.8
25	IC 4030	0	S0	16	6985	195.1165	27.9560	14.9
26	LEDA 83720	0	E	45	7015	194.6336	27.4563	14.9
27	LEDA 83677	0	E	78	6176	194.2948	27.4049	14.9
28	RB 045	0	E	19	6685	194.9322	27.9947	15.0
29	CGCG 160–233	0	E	25	6925	194.9265	27.9247	15.0
30	LEDA 83721	0	S0	46	6985	194.6381	27.3644	15.0
31	RB 064	0	S0/a	25	7705	194.9861	27.9300	15.1
32	Mrk 057	0	Sc	59	7675	194.6553	27.1766	15.1
33	RB 116	0	S0/a	1	6565	195.1860	28.1006	15.2
34	RB 022	0	E	13	5636	194.8697	28.0405	15.3
35	RB 046	0	E	18,19	6895	194.9342	27.9584	15.4
36	RB 040	0	S0	19	8034	194.9152	27.9539	15.4
37	RB 094	0	S0s	23	5126	195.0782	27.9371	15.4
38	RB 214	0	S0	75	6925	194.7401	27.7854	15.4
39	IC 4011	0	E	10	7225	195.0266	28.0041	15.5
40	KUG 1254+274	0	Sbc	63	7195	194.1443	27.2276	15.5
41	RB 074	0	S0	10	5906	195.0225	28.0245	15.6
42	RB 038	0	Sa	19	6805	194.9097	27.9872	15.7
43	RB 042	0	S0	19	7585	194.9178	27.9682	15.7
44	LEDA 83675	0	Sa	90	8304	194.2681	27.5259	15.9
45	IC 4012	0	E	3	7225	194.0333	28.0786	16.0
46	RB 091	0	S0	3	6116	195.0709	28.0639	16.0
47	RB 031	0	E	33	6266	194.8970	27.8636	16.0
48	RB 055	0	E	25	9773	194.9588	27.9248	16.1
49	SDSS J130051.15+280249.6	0	E	8	6446	195.2132	28.0471	16.2
50	RB 226	0	E	14	7195	194.7894	28.0409	16.4
51	SDSS J125931.13+275717.6	0	S0	19	7075	194.8797	27.9549	16.5
52	SDSS J125825.29+271159.9	0	Sa	59	8004	194.6054	27.2000	16.6
53	RB 263	0	S0	14	8004	194.7699	28.0504	16.7
54	SDSS J125820.53+272545.7	0	S0	45	7525	194.5856	27.4294	16.7
55	SDSS J130011.13+280354.8	0	S0	3	7315	195.0464	28.0653	16.8
56	RB 267	0	E	14	6895	194.7981	28.0093	16.8
57	LEDA 126756	0	Sa	23	7915	195.1034	27.9266	16.8
58	CcGV9a	0	S0	9,10	6206	195.0787	28.0093	16.9
59	RB 095	0	S0	23	4857	195.0903	27.8986	16.9
60	LEDA 1801787	0	Sbc	63	6056	194.0990	27.2340	16.9
61	RB 210	0	E	75	6476	194.7277	27.7956	16.9
62	RB 037	0	Sa	19	4947	194.9083	28.0010	17.0

ID	Name	Rating	Type	Visit	$V_h$ (km s <sup>-1</sup> )	$\alpha$ (J2000)	$\delta$ (J2000)	$m_{F814}$
63	RB 071	0	S0	24	6835	195.0040	27.9454	17.0
64	SDSS J125957.43+275556.6	0	Sc	25	4557	194.9893	27.9324	17.0
65	SDSS J130018.54+280549.7	0	dE	3	7795	195.0773	28.0972	17.1
66	LEDA 126789	0	E	33	4647	194.8829	27.8613	17.1
67	SDSS J130041.19+280242.4	0	dE	8	8604	195.1717	28.0451	17.2
68	SDSS J130034.42+275604.9	0	S0	22	8724	195.1435	27.9347	17.2
69	RB 068	0	S0	24	6146	194.9978	27.9406	17.2
70	SDSS J130013.42+280311.8	0	S0	10	8124	195.0559	28.0533	17.3
71	SDSS J130035.42+275633.9	0	S0	22	6925	195.1458	27.9428	17.3
72	LEDA 126815	0	E	75	6655	194.6898	27.7539	17.3
73	LEDA 126754	0	E	2	5156	195.1290	28.1086	17.4
74	LEDA 126815	0	dE	3	9983	195.0764	28.0593	17.4
75	RB 199	0	dI	75	8694	194.6775	27.7605	17.4
76	SDSS J125950.18+275445.4	0	E	25	7285	194.9591	27.9126	17.5
77	SDSS J125937.00+280106.9	0	E	12	7195	194.9042	28.0186	17.7
78	SDSS J130022.90+275515.1	0	dE	23	5476	195.0956	27.9208	17.7
79	SDSS J125948.59+275857.8	0	E	18	5396	194.9525	27.9827	17.8
80	SDSS J125946.93+275930.8	0	S0	18	8364	194.9456	27.9919	17.8
81	SDSS J130007.12+275551.4	0	E	24	7765	195.0297	27.9310	17.8
82	SDSS J125926.45+275124.7	0	E	33	4977	194.8602	27.8569	17.8
83	SDSS J125815.27+272752.9	0	S0	45	7615	194.5636	27.4647	17.8
84	SDSS J125930.25+280115.0	0	E	13	7195	194.8761	28.0209	17.9
85	SDSS J130009.46+275456.3	3	E	24		195.0398	27.9156	17.9
86	SDSS J125831.66+272342.1	0	Sc	46	7495	194.6317	27.3950	17.9
87	SDSS J130039.10+280035.5	0	dE	8	5785	195.1627	28.0099	18.1
88	SDSS J130026.16+280032.0	0	E	9	5546	195.1090	28.0089	18.1
89	SDSS J125914.43+280217.3	1	dE,N	14		194.8102	28.0381	18.1
90	SDSS J130017.64+275915.1	0	E	16	5966	195.0735	27.9876	18.1
91	SDSS J125953.93+275813.7	0	E	18	6745	194.9747	27.9705	18.1
92	CcGV19a	0	E	19		194.9049	27.9722	18.1
93	SDSS J125937.20+275213.6	0	E	33	6326	194.9053	27.8705	18.1
94	SDSS J125928.50+280109.3	0	E	13	5996	194.8688	28.0193	18.2
95	SDSS J125955.69+275503.7	0	dE	25	6625	194.9821	27.9177	18.2
96	SDSS J125636.78+271247.8	2	dE,N	63		194.1530	27.2131	18.2
97	SDSS J125635.49+271430.3	0	dE	63	5606	194.1479	27.2418	18.2
98	RB 110	0	dE,N	8	7615	195.1607	28.0160	18.3
99	SDSS J125946.71+280000.4	2	dE,N	12		194.9447	28.0002	18.3
100	SDSS J125844.31+274501.0	3	E	75		194.6845	27.7503	18.3
101	SDSS J130000.97+275929.5	0	dE	18	7525	195.0041	27.9916	18.4
102	SDSS J125844.58+274458.2	3	S0	75		194.6857	27.7495	18.4
103	SDSS J130042.86+280313.8	0	dE	8	6775	195.1786	28.0538	18.5
104		0	dE,N	13	6296	194.8784	28.0421	18.5
105	SDSS J130033.33+275849.3	0	dE	15	5156	195.1389	27.9804	18.5
106	SDSS J130036.67+275427.5	2	dE,N	22		195.1527	27.9076	18.5
107		3	dE,N	25		194.9580	27.9090	18.5
108	SDSS J130025.97+280344.6	0	dE,N	2	7495	195.1083	28.0626	18.6
109		0	dE,N	63	9054	194.1588	27.2178	18.6
110	SDSS J130032.61+280331.4	0	dE,N	2	7375	195.1359	28.0589	18.7
111	SDSS J130048.04+280557.2	0	E	1	6236	195.2001	28.0992	18.8
112		1	dE,N	10		195.0238	28.0259	18.8
113	SDSS J130036.58+275552.2	0	dE,N	22	5906	195.1524	27.9312	18.8
114		0	dE,N	78	7345	194.3051	27.4103	18.8
115	SDSS J130011.41+275436.4	0	dE	24	7285	195.0476	27.9101	18.9
116	SDSS J125942.36+280158.5	0	dE,N	12	7885	194.9265	28.0329	19.0
117	SDSS J130022.65+275754.9	0	dE,N	12,13	7105	194.8885	28.0313	19.0
118	SDSS J130022.65+275754.9	0	E	16	5216	195.0944	27.9653	19.0
119	SDSS J130005.34+275628.9	2	dE	24		195.0224	27.9413	19.0
120	SDSS J125844.37+274740.9	0	dE	75	6176	194.6849	27.7947	19.0
121	SDSS J130027.57+280323.9	0	dE	9	5786	195.1149	28.0566	19.1
122	SDSS J130004.03+280030.7	0	E	10	6386	195.0168	28.0085	19.1
123	SDSS J125902.43+280021.3	0	E	14	7974	194.7602	28.0059	19.1
124	CcGV9b	0	E	9	6425	195.1137	28.0092	19.2

ID	Name	Rating	Type	Visit	$V_h$ (km s <sup>-1</sup> )	$\alpha$ (J2000)	$\delta$ (J2000)	$m_{F814W}$
125	SDSS J130018.70+275512.6	0	dE	23	6925	195.0779	27.9202	19.2
126	SDSS J125711.01+273142.2	1	dE,N	90		194.2960	27.5286	19.2
127	CcGV1	0	E	1	6775	195.1986	28.0927	19.3
128	SDSS J130044.10+280215.4	0	dE,N	8	8756	195.1836	28.0376	19.3
129	SDSS J125921.57+280101.6	0	dE	13	6655	194.8399	28.0171	19.3
130	SDSS J125712.27+272313.0	2	dE	78		194.3011	27.3871	19.3
131	SDSS J130014.15+280407.4	0	dE	3	7255	195.0590	28.0687	19.4
132	SDSS J125712.27+272313.0	2	dE,N	12		194.9287	28.0341	19.4
133	SDSS J125943.53+275620.6	0	dE,N	25	7075	194.9314	27.9391	19.4
134		0	dE	59	7405	194.6182	27.2209	19.4
135	SDSS J125905.94+280228.8	0	dE,N	14	8154	194.7747	28.0414	19.5
136	SDSS J130016.68+275638.9	0	dE,N	23	5126	195.0694	27.9440	19.5
137		3	Sdm	45		194.5622	27.4627	19.5
138	SDSS J130042.51+280325.4	0	E	1	5670	195.1771	28.0570	19.6
139	SDSS J130020.39+280413.9	0	dE	3	7045	195.0850	28.0706	19.6
140	SDSS J130037.30+275441.0	0	dE,N	22	6086	195.1554	27.9114	19.6
141	SDSS J125958.22+275410.8	0	dE	24	7315	194.9926	27.9030	19.6
142	SDSS J130032.51+280201.4	0	dE	9	6356	195.1355	28.0337	19.7
143	SDSS J125955.93+275748.6	0	dE	18	6955	194.9831	27.9635	19.7
144	SDSS J130016.96+275416.0	0	E	23	9084	195.0707	27.9045	19.7
145	SDSS J130023.47+280301.9	0	dE	9	6925	195.0977	28.0505	19.8
146	SDSS J130032.48+275833.2	0	dE,N	15	8208	195.1353	27.9759	19.8
147	SDSS J130027.87+275916.3	0	dE	16	9593	195.1162	27.9879	19.8
148		1	VLSB	1		195.2102	28.0656	19.9
149		1	VLSB	9		195.1340	28.0376	19.9
150	CcGV19b	0	E	19	7075	194.9133	27.9985	19.9
151	SDSS J125636.63+271503.6	2	dE	63		194.1525	27.2509	19.9
152	SDSS J130020.39+280413.9	0	dE	3	5156	195.0655	28.0977	20.0
153	SDSS J130005.76+280212.1	2	dE,N	10		195.0239	28.0367	20.0
154	SDSS J130032.96+275406.6	2	dE,N	22		195.1373	27.9018	20.0
155	CcGV18	0	E	18	6535	194.9996	27.9894	20.1
156		2	dE	19		194.9022	27.9608	20.1
157	SDSS J130003.18+275648.3	3	dE,N	24		195.0135	27.9465	20.1
158		2	dE,N	25		194.9245	27.9262	20.1
159	SDSS J125927.22+275257.0	0	dE	33	6745	194.8634	27.8825	20.1
160	SDSS J125951.46+275935.4	0	dE	18	7195	194.9645	27.9932	20.2
161	SDSS J125930.83+275810.2	0	dE	19	5426	194.8785	27.9695	20.2
162		2	dE,N	22		195.1479	27.9438	20.2
163	SDSS J125945.55+280313.4	2	dE,N	12		194.9397	28.0538	20.3
164	SDSS J130031.92+275711.2	0	dE	15	5876	195.1330	27.9531	20.3
165		0	dE,N	22	6748	195.1499	27.9181	20.3
166		2	dE,N	25		194.9616	27.9206	20.3
167		2	dE,N	33		194.8487	27.8451	20.3
168	SDSS J125845.91+274655.5	2	dE,N	75		194.6912	27.7823	20.3
169	SDSS J125920.90+280057.5	0	E	13	6805	194.8371	28.0160	20.4
170	SDSS J130024.85+275921.8	0	dE,N	16	9081	195.1037	27.9895	20.4
171	SDSS J125942.92+275954.6	0	dE,N	19	8274	194.9288	27.9984	20.4
172	SDSS J130018.41+275516.9	0	dE	23	7899	195.0767	27.9212	20.4
173		2	dE	25		194.9535	27.9155	20.4
174	SDSS J125853.08+274741.8	2	dE,N	75		194.7211	27.7949	20.4
175	SDSS J125708.35+272923.9	0	E	90	7555	194.2848	27.4900	20.4
176	SDSS J130027.57+280323.9	0	dE	2	5786	195.1151	28.0567	20.5
177	CcGV12	0	E	12	7721	194.9263	28.0153	20.5
178		0	S0	18	8814	194.9988	27.9983	20.5
179	SDSS J125959.08+275841.4	3	dE,N	18		194.9961	27.9782	20.5
180		1	VLSB	19		194.9158	27.9905	20.5
181	SDSS J130019.08+280508.9	2	dE	3		195.0795	28.0858	20.6
182	SDSS J125915.99+280109.1	3	dE	14		194.8165	28.0193	20.6
183		0	dE	23	6706	195.1043	27.9437	20.6
184	SDSS J130016.37+275522.2	0	dE,N	23	4439	195.0681	27.9227	20.6
185		3	dE	23		195.0918	27.8987	20.6
186	SDSS J130002.70+275645.1	2	dE	24		195.0110	27.9457	20.6

ID	Name	Rating	Type	Visit	$V_h$ (km s <sup>-1</sup> )	$\alpha$ (J2000)	$\delta$ (J2000)	$m_{F814W}$
187	SDSS J130015.68+280146.3	0	dE,N	10	6760	195.0653	28.0295	20.7
188		1	VLSB	22		195.1691	27.9337	20.7
189	SDSS J130010.38+275617.0	0	E	24	7285	195.0432	27.9380	20.7
190		1	VLSB	25		194.9367	27.9268	20.7
191		2	dE/I	25		194.9200	27.9118	20.7
192	SDSS J125856.95+274719.9	2	dE	75		194.7373	27.7889	20.7
193	SDSS J130011.81+280504.0	1	dE,N	3		195.0492	28.0837	20.8
194	SDSS J130030.94+280312.8	0	dE,N	9	7208	195.1288	28.0535	20.8
195		3	dE,N	12		194.9056	28.0365	20.8
196	SDSS J130034.32+275817.6	0	dE	15	7686	195.1429	27.9714	20.8
197	SDSS J125934.39+275942.9	0	dE,N	19	5007	194.8931	27.9953	20.8
198	SDSS J125700.84+273015.7	3	dE	90		194.2535	27.5044	20.8
199	SDSS J130039.76+280601.9	1	VLSB	2		195.1658	28.1008	20.9
200	SDSS J130021.38+280327.3	0	dE	3	7594	195.0889	28.0574	20.9
201	SDSS J130020.27+280453.2	0	dE	3	8004	195.0846	28.0813	20.9
202	SDSS J125928.55+280305.2	3	dE,N	13		194.8690	28.0516	20.9
203	SDSS J125850.42+274445.7	2	dE,N	75		194.7100	27.7460	20.9
204	SDSS J130039.35+280411.0	0	dE,N	1	6469	195.1640	28.0697	21.0
205	SDSS J130026.88+280450.7	2	dE,N	2		195.1121	28.0810	21.0
206	SDSS J130017.24+280547.2	2	dE	3		195.0718	28.0964	21.0
207		0	dE/I	10	5126	195.0562	28.0373	21.0
208	SDSS J130047.53+275829.9	0	dE/I	15	5660	195.1980	27.9749	21.0
209		2	dE	15		195.1595	28.0024	21.0
210	SDSS J130039.32+275748.4	0	dE,N	15	6357	195.1636	27.9633	21.0
211		1	VLSB	16		195.1217	27.9902	21.0
212		2	dE,N	22		195.1648	27.8972	21.0
213		3	dE,N	24		195.0198	27.9045	21.0
214	SDSS J130007.04+275416.8	2	dE,N	24		195.0293	27.9047	21.0
215		3	dE,N	25		194.9599	27.9216	21.0
216	SDSS J130011.81+280504.0	2	dE,N	3		195.0490	28.0846	21.1
217	SDSS J125951.81+275726.3	0	dE,N	18	5666	194.9659	27.9572	21.1
218		2	dE	23		195.0737	27.9368	21.1
219		2	dE,N	25		194.9864	27.9377	21.1
220		1	VLSB	1		195.2142	28.0738	21.2
221		2	dE,N	13		194.8561	28.0365	21.2
222		0	dE,N	16	7081	195.1166	27.9983	21.2
223	SDSS J126944.76+275807.1	0	dE	18,19	9623	194.9363	27.9685	21.2
224	SDSS J125931.19+275754.2	0	dI	19	7435	194.8800	27.9651	21.2
225		2	dE	25		194.9678	27.9218	21.2
226		2	VLSB	33		194.8649	27.8714	21.2
227	SDSS J125843.28+274721.1	2	dE	75		194.6802	27.7893	21.2
228	SDSS J130039.05+280437.1	3	dE,N	1,2		195.1628	28.0770	21.3
229		2	dE	3		195.0693	28.0812	21.3
230	SDSS J130022.01+280220.9	0	dE,N	9	7839	195.0914	28.0384	21.3
231		2	dE	33		194.8622	27.8601	21.3
232	SDSS J125700.89+273155.1	2	dE,N	90		194.2537	27.5322	21.3
233	SDSS J130030.94+280312.8	0	dE,N	2	7395	195.1289	28.0537	21.4
234	SDSS J130029.81+280401.0	3	dE,N	2		195.1244	28.0670	21.4
235	SDSS J130031.97+280125.1	0	dE,N	9	7990	195.1322	28.0227	21.4
236	SDSS J130017.61+275927.3	2	dE	16	4993	195.0735	27.9912	21.4
237		0	dE,N	16	5220	195.1240	27.9686	21.4
238	SDSS J130004.04+275342.7	2	dE,N	24		195.0168	27.8951	21.4
239	SDSS J130030.05+280134.8	0	dE	9	6455	195.1249	28.0264	21.5
240	SDSS J125941.47+275439.6	3	dE,N	25		194.9228	27.9109	21.5
241		3	dE,N	13		194.8752	28.0439	21.6
242		0	dE	16	6879	195.0822	27.9848	21.6
243	SDSS J130000.97+275929.5	1	dE,N	18		195.0042	27.9929	21.6
244	SDSS J125952.18+275946.3	2	dE,N	18		194.9674	27.9962	21.6
245	SDSS J125856.78+274644.5	3	dE	75		194.7366	27.7789	21.6
246	SDSS J130007.76+280052.1	3	dE/I	10		195.0321	28.0143	21.7
247		3	dE,N	13		194.8776	28.0223	21.7
248	SDSS J130037.83+275840.9	0	dE	15	4684	195.1576	27.9779	21.7

ID	Name	Rating	Type	Visit	$V_h$ (km s <sup>-1</sup> )	$\alpha$ (J2000)	$\delta$ (J2000)	$m_{F814W}$
249		1	dE	18		194.9619	27.9602	21.7
250	SDSS J125943.95+275802.0	2	dE,N	19	7705	194.9330	27.9672	21.7
251		2	dE	33		194.9011	27.8853	21.7
252	SDSS J125932.99+275126.3	3	dE	33		194.8774	27.8565	21.7
253	SDSS J130009.24+280359.6	3	dE,N	3		195.0385	28.0664	21.8
254	SDSS J130018.27+275817.6	0	dE	16	4723	195.0762	27.9716	21.8
255	SDSS J125945.39+275829.1	2	dE,N	18,19		194.9388	27.9746	21.8
256		2	dE,N	19		194.9108	27.9496	21.8
257		1	VLSB	22		195.1403	27.9234	21.8
258		0	dE,N	23	5805	195.0676	27.9121	21.8
259	SDSS J125833.56+272420.6	3	dE,N	46		194.6397	27.4060	21.8
260		2	VLSB	13		194.8690	28.0228	21.9
261		2	dE	13		194.8610	28.0238	21.9
262		0	dE	15	4693	195.1822	27.9890	21.9
263		1	VLSB	16		195.0957	27.9775	21.9
264		0	dE,N	16	6156	195.0969	27.9970	21.9
265		2	dE/I	1		195.1965	28.0858	22.0
266		0	dE	3	7195	195.0805	28.0726	22.0
267		2	dE,N	9,10		195.0843	28.0339	22.0
268		2	dE,N	18		194.9855	27.9859	22.0
269		2	dE	19		194.8825	28.0015	22.0
270		0	dE	19	8694	194.8821	27.9634	22.0
271		3	dE/I	24		195.0161	27.9338	22.0
272	SDSS J125936.48+275108.0	2	dE	33		194.9018	27.8521	22.0
273	SDSS J125936.43+275101.7	2	dE,N	33		194.9015	27.8505	22.0
274	SDSS J125832.93+272406.5	3	dE,N	46		194.6370	27.4020	22.0
275	SDSS J125824.72+271128.8	3	dE	59		194.6030	27.1911	22.0
276	SDSS J130037.05+280544.7	1	VLSB	2		195.1536	28.0962	22.1
277		3	dE/I	2		195.1519	28.0896	22.1
278		2	dE	3		195.0615	28.0815	22.1
279		2	dE	10		195.0402	28.0307	22.1
280		0	dE,N	10	7975	195.0591	28.0073	22.1
281	SDSS J125939.09+275932.4	0	dE	19	6955	194.9129	27.9924	22.1
282		2	VLSB	19		194.9204	27.9548	22.1
283		3	dE	22		195.1553	27.9236	22.1
284		2	dE	23		195.0766	27.9250	22.1
285		3	dE/I	63		194.1613	27.2202	22.1
286		2	dE,N	1		195.2205	28.0765	22.2
287		0	dE,N	1	7786	195.1913	28.0597	22.2
288		3	dE	2		195.1355	28.0606	22.2
289	SDSS J130022.84+280057.1	0	dE,N	9	9142	195.0951	28.0157	22.2
290		3	dE,N	12		194.9351	28.0413	22.2
291		2	dE,N	19		194.9068	27.9686	22.2
292		2	dE/I	24		195.0428	27.9401	22.2
293	SDSS J125637.64+271244.0	3	dI	63		194.1568	27.2120	22.2
294		2	dE,N	1		195.2053	28.0768	22.3
295		2	dE/I	10		195.0450	28.0331	22.3
296		2	dE,N	12		194.8971	28.0244	22.3
297		0	dE/I	13	5216	194.8585	28.0178	22.3
298		1	VLSB	19		194.9244	27.9467	22.3
299		2	dE,N	22		195.1240	27.9319	22.3
300		2	dE	23		195.0919	27.9118	22.3
301		1	dE	75		194.7321	27.7579	22.3
302		3	dE,N	75		194.6836	27.7798	22.3
303		0	dE,N	1	6518	195.2126	28.0631	22.4
304		1	VLSB	3		195.0939	28.1043	22.4
305		3	dE,N	10		195.0617	28.0085	22.4
306		2	dE/I	12		194.9083	28.0152	22.4
307		3	dE/I	13		194.8796	28.0525	22.4
308		2	dE	18,19		194.9369	27.9721	22.4
309		0	dE	19	5906	194.9086	27.9490	22.4
310		1	VLSB	23		195.0560	27.9020	22.4

ID	Name	Rating	Type	Visit	$V_h$ (km s <sup>-1</sup> )	$\alpha$ (J2000)	$\delta$ (J2000)	$m_{F814W}$
311		2	dE,N	24		195.0331	27.9431	22.4
312		3	dE,N	24		195.0102	27.9497	22.4
313		3	dE	24		195.0385	27.9076	22.4
314		3	dE	33		194.9008	27.8814	22.4
315		2	dE,N	45		194.6363	27.4596	22.4
316		2	dE,N	1		195.1769	28.0655	22.5
317		3	dE/I	2		195.1098	28.1098	22.5
318		2	dE,N	3		195.0814	28.1001	22.5
319		3	dE,N	3		195.0826	28.0658	22.5
320		2	dE	10		195.0585	28.0298	22.5
321		2	dE,N	10		195.0286	28.0321	22.5
322		2	dE	10		195.0524	28.0085	22.5
323		2	dE	16		195.1377	27.9957	22.5
324		3	dE	18		195.0002	27.9784	22.5
325		2	dE,N	19		194.9121	27.9789	22.5
326		2	dE,N	19		194.8870	27.9666	22.5
327		3	dE	22		195.1334	27.9519	22.5
328		2	dE,N	33		194.8748	27.8967	22.5
329		3	dE/I	59		194.6341	27.1726	22.5
330	SDSS J130035.98+280550.7	2	dE,N	2		195.1501	28.0975	22.6
331		3	dE/I	3		195.0898	28.1079	22.6
332		3	dE/I	9		195.1180	28.0299	22.6
333		3	dE/I	10		195.0612	27.9988	22.6
334		2	dE,N	18		194.9688	27.9734	22.6
335		2	dE	23		195.0904	27.9472	22.6
336		2	dE,N	23		195.1189	27.9438	22.6
337		3	dE/I	24		195.0286	27.9083	22.6
338		3	dE	24		195.0051	27.9435	22.6
339		0	dE	25	7105	194.9333	27.9375	22.6
340		2	dE	33		194.8538	27.8889	22.6
341		1	dE/I	75		194.7270	27.7622	22.6
342		3	dI	78		194.2910	27.4023	22.6
343		1	VLSB	1		195.1793	28.1044	22.7
344		2	dE	2		195.1044	28.0582	22.7
345	SDSS J130011.95+280402.4	0	dE/I	3	6895	195.0497	28.0674	22.7
346		3	dE	8		195.2096	28.0327	22.7
347		3	dE	10		195.0749	28.0502	22.7
348		3	dE	10		195.0623	28.0380	22.7
349		2	VLSB	12		194.9267	28.0107	22.7
350		3	dE,N	14		194.8067	28.0069	22.7
351		3	dE/I	22		195.1562	27.8983	22.7
352		2	VLSB	33		194.8811	27.8688	22.7
353		2	VLSB	46		194.6238	27.3821	22.7
354		2	dE/I	63		194.1527	27.2486	22.7
355		2	dE	3		195.0922	28.0673	22.8
356		3	dE,N	9		195.1053	28.0279	22.8
357		3	dE	9		195.1448	28.0239	22.8
358		1	VLSB	12		194.9456	28.0307	22.8
359		3	dE,N	12		194.9386	28.0501	22.8
360		3	dE,N	13		194.8496	28.0367	22.8
361		0	dE,N	19	7105	194.8967	27.9805	22.8
362		2	VLSB	25		194.9266	27.9147	22.8
363		3	dE	33		194.8716	27.8620	22.8
364		3	dE/I	3		195.0693	28.0907	22.9
365		2	dE	9		195.1042	28.0578	22.9
366		3	dE,N	10		195.0748	27.9966	22.9
367		2	dE/I	12		194.9099	28.0571	22.9
368		2	dE,N	23		195.0817	27.9169	22.9
369		2	dE/I	24		195.0152	27.9201	22.9
370		2	dE/I	24		195.0305	27.9064	22.9
371		3	dE,N	33		194.8817	27.8669	22.9
372		3	dE	3		195.0613	28.0772	23.0

ID	Name	Rating	Type	Visit	$V_h$ (km s <sup>-1</sup> )	$\alpha$ (J2000)	$\delta$ (J2000)	$m_{F814W}$
373		2	dE/I	9		195.1242	28.0409	23.0
374		1	VLSB	12		194.9007	28.0550	23.0
375		3	dE/I	12		194.9358	28.0369	23.0
376		3	dE	15		195.1753	27.9486	23.0
377		2	dE	19		194.9358	27.9742	23.0
378		2	dE	19		194.9130	27.9605	23.0
379		3	dE	9		195.1403	28.0240	23.1
380		1	VLSB	12		194.9592	28.0491	23.1
381		2	dE	13		194.8588	28.0036	23.1
382		3	dI	13		194.8799	28.0228	23.1
383		1	VLSB	16		195.1076	27.9552	23.1
384		3	dE,N	19		194.8864	27.9906	23.1
385		2	dE	22		195.1662	27.9365	23.1
386		2	dE/I	24		195.0152	27.9202	23.1
387		2	dE,N	25		194.9722	27.9407	23.1
388		3	dE/I	33		194.8654	27.8980	23.1
389		3	dE/I	75		194.7062	27.7567	23.1
390		3	dE	78		194.2661	27.4136	23.1
391		3	dI	8		195.1565	28.0165	23.2
392		3	dE	14		194.7958	28.0241	23.2
393		1	VLSB	15		195.1856	27.9609	23.2
394		2	VLSB	15		195.1826	27.9524	23.2
395		3	dE	18,19		194.9404	27.9781	23.2
396		3	dE	19		194.9141	27.9573	23.2
397		3	dE,N	23		195.0946	27.9272	23.2
398		3	dE/I	25		194.9754	27.9142	23.2
399		2	dE/I	75		194.7108	27.7478	23.2
400		3	VLSB	75		194.6802	27.7864	23.2
401		3	dE,N	3		195.0608	28.0873	23.3
402		2	dE/I	8		195.1682	28.0491	23.3
403		3	dE/I	10		195.0525	28.0519	23.3
404		3	dE,N	16		195.0734	27.9817	23.3
405		2	dE	18		194.9859	27.9837	23.3
406		2	dE	22		195.1833	27.9227	23.3
407		2	VLSB	23		195.0971	27.8958	23.3
408		2	dE/I	24		195.0383	27.8974	23.3
409		2	dE	25		194.9816	27.9138	23.3
410		2	dE/I	25		194.9815	27.9140	23.3
411		2	dE,N	25		194.9813	27.9061	23.3
412		3	dE/I	25		194.9814	27.9372	23.3
413		2	dE	10		195.0273	28.0281	23.4
414		3	VLSB	14		194.7608	28.0294	23.4
415		3	dE/I	14		194.7809	28.0407	23.4
416		2	VLSB	15		195.1411	27.9617	23.4
417		2	VLSB	18		194.9922	27.9690	23.4
418		3	dE/I	23		195.0689	27.9297	23.4
419		2	VLSB	24		195.0338	27.8924	23.4
420		2	dE/I	33		194.8404	27.8480	23.4
421		3	dE,N	63		194.1062	27.2213	23.4
422		3	VLSB	14		194.7885	28.0094	23.5
423		1	VLSB	15		195.1985	27.9831	23.5
424		3	dE,N	16		195.1192	27.9441	23.5
425		2	VLSB	18		194.9964	27.9958	23.5
426		3	dE	19		194.9260	27.9769	23.5
427		2	VLSB	22		195.1702	27.9150	23.5
428		3	dE,N	23		195.0955	27.9278	23.5
429		3	dE,N	24		195.0141	27.9009	23.5
430		3	dE/I	90		194.3106	27.5377	23.5
431		3	dE,N	10		195.0572	28.0424	23.6
432		2	VLSB	10		195.0719	28.0163	23.6
433		3	VLSB	14		194.8175	28.0446	23.6
434		3	dE	19		194.8836	27.9890	23.6

ID	Name	Rating	Type	Visit	$V_h$ (km s $^{-1}$ )	$\alpha$ (J2000)	$\delta$ (J2000)	$m_{F814W}$
435		3	dE	19		194.9120	27.9627	23.6
436		3	dE,N	19		194.9232	27.9856	23.6
437		3	dE/I	23		195.1094	27.9356	23.6
438		3	dE/I	63		194.1381	27.2288	23.6
439		3	dI	78		194.2843	27.4259	23.6
440		2	dE/I	3		195.0489	28.0712	23.7
441		2	dE	10		195.0453	28.0202	23.7
442		2	dE	10		195.0600	28.0244	23.7
443		3	dE/I	14		194.7762	28.0329	23.7
444		3	dE/I	18		195.0013	27.9960	23.7
445		3	dE,N	18		194.9593	27.9873	23.7
446		2	VLSB	19		194.9312	27.9680	23.7
447		3	VLSB	22		195.1673	27.9073	23.7
448		2	dE/I	24		194.9916	27.9138	23.7
449		2	dE/I	25		194.9754	27.9141	23.7
450		2	dE/I	33		194.8624	27.8920	23.7
451		2	dE/I	3		195.0616	28.0817	23.8
452		2	VLSB	10		195.0735	28.0328	23.8
453		3	dE/I	16		195.1241	27.9509	23.8
454		3	dE/I	18		195.0004	27.9845	23.8
455		3	dE/I	18		194.9464	27.9557	23.8
456		3	dE/I	19		194.9002	27.9655	23.8
457		3	dE/I	46		194.6680	27.3822	23.8
458		3	dE/I	1		195.1907	28.1073	23.9
459		3	dE/I	10		195.0471	28.0030	23.9
460		2	dE	25		194.9401	27.9172	23.9
461		3	dE/I	9		195.1323	28.0496	24.0
462		3	dE/I	15		195.1942	27.9725	24.0
463		2	VLSB	16		195.1087	27.9622	24.0
464		3	dE,N	22		195.1404	27.9205	24.0
465		2	dE/I	33		194.8613	27.9063	24.0
466		3	VLSB	45		194.5928	27.4756	24.0
467		3	dE/I	90		194.2645	27.5376	24.0

$$M_I = m_I - DM - A_I$$

where DM is the distance modulus, assumed to be 35.0 mag,  $m_I$  is the apparent magnitude and  $A_I$  is the Galactic extinction, assumed to be zero in the direction of the Coma Cluster (Schegel, Finkbeiner & Davis 1998). Magnitudes are in the AB system (note that  $I_{\text{Vega}} = I_{\text{AB}} - 0.45$ ; Blanton & Roweis 2007). Corrections for gravitational lensing by the cluster dark matter and from absorption by intracluster dust are assumed negligible (Bernstein et al. 1995).

In Figure 3 we present the LF for the sample of galaxies in Table 3. In this section we describe the properties of the galaxies in each magnitude range and determine the type-specific LF and the radial dependence of the LF. Finally we compare our results to previous determinations of the Coma Cluster LF and to the LF in other clusters.

The uncertainties shown in Figure 3 come from counting statistics. Most of the time these are much larger than the uncertainties due to membership assignments. The exception is the final ( $M_I = -11.25$  mag) point where the majority of galaxies are rated 3. Motivated by this and by the results of the *LRIS* program (Chiboucas et al. 2010), we estimate the underlying LF by considering the contribution of all galaxies rated 0 – 2 and 50 % of galaxies rated 3.

Uncertainties come from counting statistics except for the  $M_I = -11.25$  point where they were computed assuming a lower limit where none of the galaxies rated 3 are members (note that the fraction 50% of galaxies rated 3 that *LRIS* found to be members is appropriate for galaxies significantly brighter than the once in this bin).

The LF is gradually rising up to  $M_I = -13$  mag and then flattens until the limit of the survey at  $M_I = -11$  mag. The sample is large enough and the uncertainties small enough that the curvature of the LF is real. Over the magnitude range  $-17 \text{ mag} < M_I < -11 \text{ mag}$ , the LF is only marginally fit by a single power law: reduced  $\chi^2 = 1.7$  for 10 degrees of freedom, indicating a probability of 8% that the data are drawn from random from a power-law distribution. The problem is that an extrapolation of the power-law fit in the range  $-17 \text{ mag} < M_I < -13 \text{ mag}$  strongly overpredicts the number of galaxies with  $-13 \text{ mag} < M_I < -11 \text{ mag}$ .

#### 4.1 Contributions to the luminosity function

The contributions to the LF from ellipticals, lenticulars, spirals, dwarf ellipticals, dwarf irregulars and VLSB galaxies are presented in Table 5.

In this section we describe the properties of the galaxies which contribute to the LF in each magnitude range.

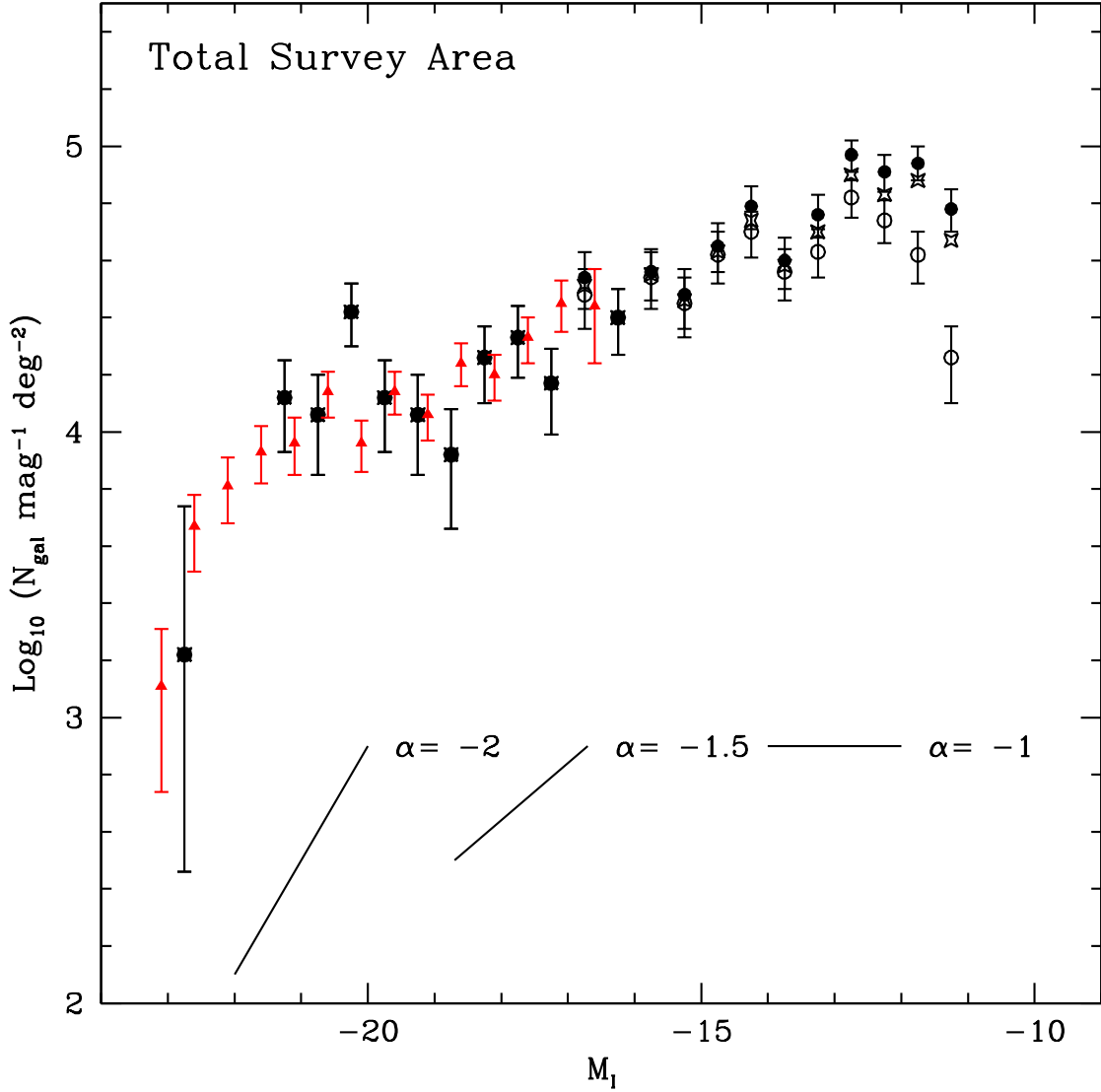


**Figure 3.** The luminosity function for the total survey area. The open symbols represent all galaxies with confirmed velocity measurements and high probability (class 1+2) members. The filled symbols represent all galaxies including those with a lower probability of membership (class 3). The stars represent the luminosity function for a sample of galaxies containing all the galaxies rated 0 – 2 and 50 per cent of the galaxies rated 3. The red triangles represent the spectroscopic luminosity function for the Coma I region of Mobasher et al. (2003). These data are scaled to the current survey to have the minimum scatter with the ACS data.

$$m_I \leq 18 \quad (M_I \leq -17)$$

The brightest galaxies in the cluster are mostly ellipticals and lenticulars. Almost all have spectroscopic velocities (the brightest galaxy without a velocity measurement has  $m_I = 17.9$  mag). Our LF is complete here, as are LFs for larger areas (e.g. Mobasher et al. 2003).

$$18 < m_I \leq 20 \quad (-17 < M_I \leq -15)$$

Most galaxies in this magnitude range are dwarf ellipticals, many of which are nucleated. There are very small numbers of VLSB galaxies and of compact elliptical galaxies. The majority of galaxies in this magnitude range have SDSS designations and velocities. Most velocities are from the SDSS,

but many are from the Hectospec observations described in Section 2.2.

$$20 < m_I \leq 22 \quad (-15 < M_I \leq -13)$$

There are 121 galaxies in this magnitude range, 36% of which have velocities and 58% of which have SDSS designations. These are mostly (87%) dwarf ellipticals, about half of which are nucleated. A small fraction (8%) are VLSB galaxies. There are two compact ellipticals in this magnitude range. The velocities mostly come from the *LRIS* observations described in Section 2.3.

$$22 < m_I \leq 23 \quad (-13 < M_I \leq -12)$$

There are 103 galaxies in this magnitude range. Of these 88 % are dwarf ellipticals. The remaining 12% are visually

**Table 5.** Contributions from different galaxy types

Magnitude range	Number	Percentage	Percentage	Percentage	Percentage	Percentage	Percentage
		E	S0	S	dE	dI	VLSB
$-23 \text{ mag} < m_I \leq -22 \text{ mag}$	1	100	0	0	0	0	0
$-22 \text{ mag} < m_I \leq -21 \text{ mag}$	9	56	22	11	0	0	0
$-21 \text{ mag} < m_I \leq -20 \text{ mag}$	21	33	52	10	0	0	0
$-20 \text{ mag} < m_I \leq -19 \text{ mag}$	16	19	44	37	0	0	0
$-19 \text{ mag} < m_I \leq -18 \text{ mag}$	18	33	44	22	0	0	0
$-18 \text{ mag} < m_I \leq -17 \text{ mag}$	22	45	27	5	18	5	0
$-17 \text{ mag} < m_I \leq -16 \text{ mag}$	34	27	0	0	74	0	0
$-16 \text{ mag} < m_I \leq -15 \text{ mag}$	34	18	0	3	73	0	6
$-15 \text{ mag} < m_I \leq -14 \text{ mag}$	61	8	2	0	83	0	8
$-14 \text{ mag} < m_I \leq -13 \text{ mag}$	60	0	0	0	92	2	7
$-13 \text{ mag} < m_I \leq -12 \text{ mag}$	103	0	0	0	86	2	12
$-12 \text{ mag} < m_I \leq -11 \text{ mag}$	89	0	0	0	75	1	24

**Table 4.** Luminosity Function for Total Survey Area

Absolute Magnitude $M_I$ mag	$\phi(M)$ N deg $^{-2}$ mag $^{-1}$
-21.25	$4.12^{+0.13}_{-0.19}$
-20.75	$4.06^{+0.14}_{-0.21}$
-20.25	$4.42^{+0.10}_{-0.12}$
-19.75	$4.12^{+0.13}_{-0.19}$
-19.25	$4.06^{+0.14}_{-0.21}$
-18.75	$3.92^{+0.16}_{-0.26}$
-18.25	$4.26^{+0.11}_{-0.16}$
-17.75	$4.33^{+0.11}_{-0.14}$
-17.25	$4.17^{+0.12}_{-0.18}$
-16.75	$4.51^{+0.09}_{-0.11}$
-16.25	$4.40^{+0.10}_{-0.13}$
-15.75	$4.55^{+0.08}_{-0.11}$
-15.25	$4.46^{+0.09}_{-0.12}$
-14.75	$4.63^{+0.08}_{-0.09}$
-14.25	$4.74^{+0.07}_{-0.08}$
-13.75	$4.58^{+0.08}_{-0.10}$
-13.25	$4.70^{+0.07}_{-0.09}$
-12.75	$4.90^{+0.06}_{-0.07}$
-12.25	$4.83^{+0.06}_{-0.07}$
-11.75	$4.88^{+0.06}_{-0.08}$
-11.25	$4.67^{+0.06}_{-0.41}$

classified as VLSB galaxies. Only 10 galaxies have velocity measurements (all from *LRIS*). The faintest of these has  $m_I = 22.8 \text{ mag}$  ( $M_I = -12.2 \text{ mag}$ ).

$23 < m_I \leq 24$  ( $-12 < M_I \leq -11$ )

There are 89 galaxies in this magnitude range. None have velocities, and 59% have rating 3 (compared to 16% for all the brighter galaxies combined). Most are dwarf ellipticals, although the majority are designated dE/I, indicating that

the signal-to-noise is not high enough that we can make the classification with confidence. A substantial minority (24%) are VLSB galaxies.

$m_I > 24$  ( $M_I > -11$ )

There are two reasons why we cannot obtain a reasonably complete sample of galaxies this faint from the current data.

Firstly, VLSB galaxies will be smaller so less of their light would be detectable above the sky background. These galaxies do not dominate the LF in the final magnitude interval but there are indications they are more common at fainter magnitudes so this may be a serious problem in this magnitude range. The detection limit of the ACS data is  $25.0 m_{F814W} \text{ mag arcsec}^{-2}$  in a  $1.0 \text{ arcsec}^2$  aperture (Carter et al. 2008). The central surface brightness of the well-studied Local Group dwarf galaxy Draco ( $M_I \sim -10 \text{ mag}$ , which is at the limit of this sample) is approximately  $24 m_{F814W} \text{ mag arcsec}^{-2}$  and its size is approximately 100 pc (0.2 arcsec at the distance of Coma) so most of its light would be above the detection limit (Hodge 1994). The galaxies which would be undetected would need to be lower in surface brightness than this.

The second reason is that we will be unable to identify the dwarf galaxies we *do* detect as cluster members. The galaxies will appear as a collection of pixels with count values significantly above sky. The problem will be to distinguish them from associations of background galaxies. For brighter galaxies the discriminant is usually the presence of a luminous matrix between the count peaks. For galaxies this faint, the luminous matrix will be below the sky noise.

## 4.2 Radial variation

The locations of all the galaxies in Table 3 are shown in Figure 4. Most of the survey area was in the cluster core but seven of the fields in Figure 1 (45,46,59,63,75,78,90) are in the cluster outskirts.

The radial variation of dwarf galaxy density in clusters can provide a direct constraint on the ingredients of galaxy formation models (Weinmann et al. 2011). However, the outer regions are too poorly sampled here to provide

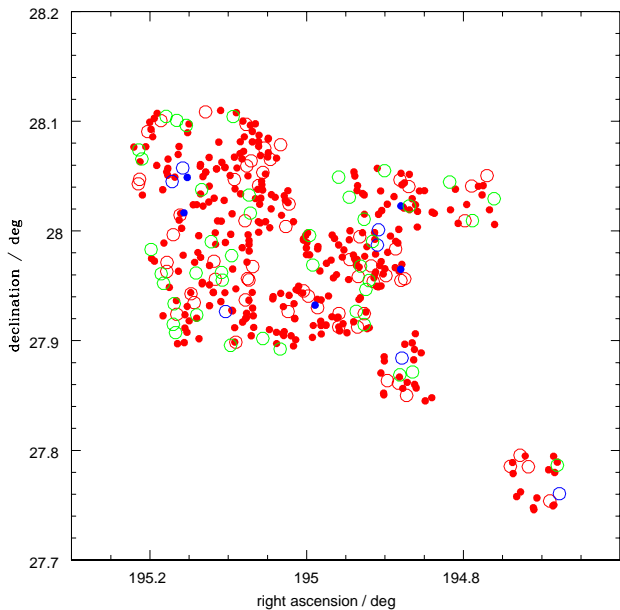


**Figure 4.** Positions of all galaxies in Table 3. The symbols have the following meanings: large red – early-type galaxies with  $M_I < -17.6$  mag, small red – early-type galaxies with  $M_I > -17.6$  mag, large blue – late-type galaxies with  $M_I < -17.6$  mag, small blue – late-type galaxies with  $M_I > -17.6$  mag, large green – VLSB galaxies.

meaningful constraints. We compare the average dwarf-to-giant ratio (DGR) for the two regions. The DGR was introduced by Phillipps et al. (1998) and Driver, Couch and Phillipps (1998) to describe the general shape of the LF in a single number. In this work we use a definition of DGR from Trentham & Tully (2009), modified from the original definition to allow for large uncertainties. The DGR here is the ratio of the number of galaxies with magnitudes between  $M_I = -17$  mag and  $M_I = -11$  mag to the number of galaxies brighter than  $M_I = -17.6$  mag. Using galaxy colours from Fukugita, Shimasaku & Ikeuchi (1995), we compute  $\text{DGR} = 6.5 \pm 1.0$  for the core and  $\text{DGR} = 2.2 \pm 0.7$  for the outer fields. The fields in the outer regions were selected to contain luminous galaxies so these fields will have a lower DGR and than is typical from fields in the outskirts. Quantitative comparisons between the two regions will require additional deep imaging over significant areas of the outskirts.

### 4.3 LF over wide magnitude range

The LF in Figure 3 and Table 4 is consistent with previous determinations (Table 1 of Milne et al. 2007) at bright magnitudes. At faint magnitudes most previous determinations of the LF comes from a background subtraction and is steep ( $\alpha = -2.3$ ; Milne et al. 2007 and  $\alpha = -3.4$ ; Yamanoi et al. 2012) so is highly inconsistent with the LF presented here. Probably there are very many more background galaxies in the direction of the cluster core than in the control fields.

The ACS data in isolation is limited because of poor counting statistics at the bright end. In Figure 5, the LF over a wide magnitude range is constructed using the SDSS

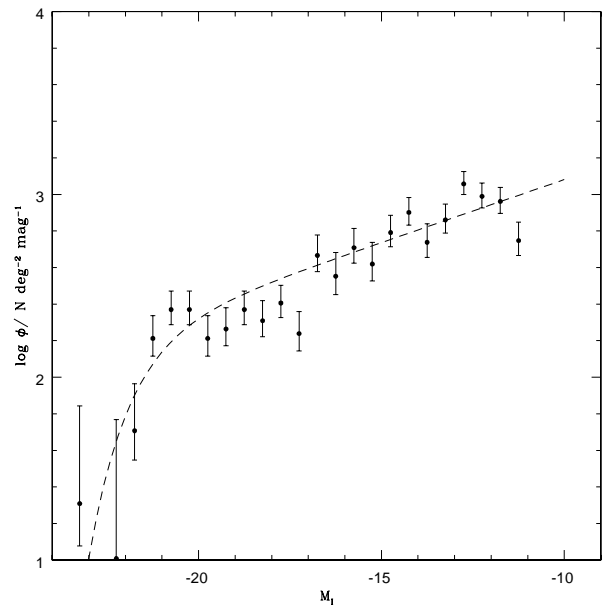


**Figure 5.** The luminosity function of the central 15 arcminutes (436 kpc) of the Coma Cluster, calculated as described in the text. The dashed line is the best-fitting Schechter function ( $M_r^* = -21.9$ ,  $\alpha^* = -1.17$ )

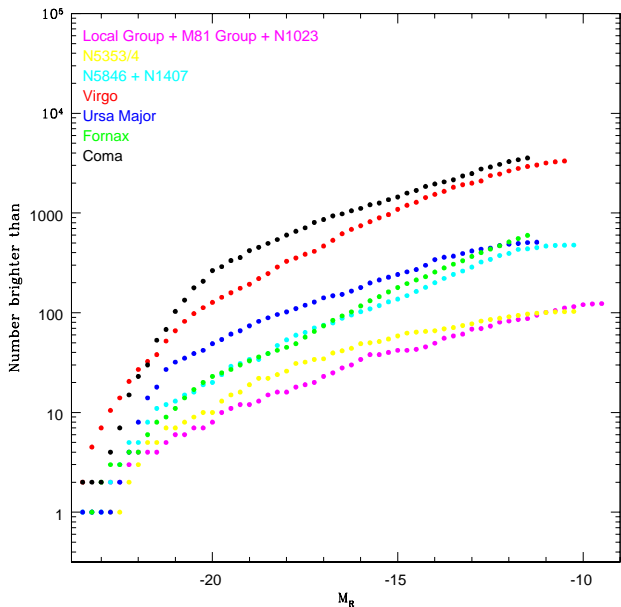
at the bright end and the ACS data at the faint end, normalized to minimise the scatter between the samples. Comparison between the SDSS and other literature surveys (see Milne et al 2007 for a list) showed that the SDSS sample was incomplete fainter than  $M_I = -18$  mag. Only galaxies brighter than this were included in computing the SDSS LF used at the bright end in Figure 5 (there were 276 galaxies).

Figure 5 also shows the best-fitting Schechter function. The greatest deviations from the function are seen at the final point where there is uncertainty due to incompleteness and membership considerations and at  $M_I = -18$  mag where there is a dip in the LF. A similar dip has also been observed in the Virgo Cluster (Rines & Geller 2008). This magnitude is also where the sample in Table 2 changes from being dominated by high-surface-brightness elliptical and lenticular galaxies low-surface-brightness dwarf elliptical galaxies.

### 4.4 Comparison with other structures

The only other environments where the LF can be determined in a similar way are in the Local Supercluster (distance  $< 33$  Mpc). The resolution of the ACS images for a cluster at the distance of Coma corresponds to the resolution of ground-based images for a cluster in the Local Supercluster.

The LFs of different environments in the Local Supercluster are described by Tully (2011). Evolved structures, characterized by large total masses that are virialized and large early-type galaxy fractions, have high DGR in the range 4 – 8 whereas uninvolved structures characterized by diffuse unvirialized structures dominated by late-type galaxies have low DGR in the range 2 – 4. Yet the total number of dwarf galaxies per unit halo mass does not vary significantly



**Figure 6.** Cumulative luminosity functions (Tully 2011) of the Coma Cluster and various structures in the Local Supercluster. The LFs of three poor spiral-rich groups are combined to improve counting statistics. These are the Local Group (van den Bergh 2000), the M81 Group (Chiboucas et al 2013) and the NGC 1023 Group (Trentham & Tully 2009). The NGC 5353/54 Group (Tully & Trentham 2008) is a knot of galaxies around an interacting pair of S0 galaxies. The NGC 5846 Group (Mahdavi et al. 2005) and the NGC 1407 Group (Trentham et al. 2006) are dense groups of early-type galaxies similar to fossil groups. The Virgo Cluster (Sandage et al. 1985, Trentham & Hodgkin 2002, Sabatini et al. 2003, Trentham & Tully 2002, Lieder et al. 2012) and the Fornax Cluster (Ferguson & Sandage 1988, Mieske et al. 2007) are dense clusters of early-type galaxies and The Ursa Major Cluster (Trentham et al. 2001, Karachentsev et al. 2013) is a diffuse accumulation of early-type and late-type galaxies. Published luminosity functions are all converted to the  $I$ -band using the colour conversions of Fukugita et al. 1995).

amongst different structures. The implication is that evolved structures are deficient in luminous galaxies. This is quantified in the cumulative luminosity function (Tully 2011) where the difference between the two LF shapes is greatest at about  $M_I = -20$ .

In Figure 6 the cumulative LF of Coma is compared to various structures in the Local Supercluster. We cannot directly determine the cumulative LF of the entire Coma Cluster (as for the other structures) due to the small ACS survey area. Instead we estimate it using the SDSS for galaxies within 90 arcminutes of NGC 4874 (there were 496 galaxies brighter than  $M_I = -18$  mag) brighter than  $M_I = -18.5$  and a scaled ACS LF fainter than this. The Coma LF differs from the other evolved environments in that there are more luminous galaxies:  $DGR = 4.0 \pm 0.2$ . This is significantly lower than the DGR in the central region (5.1) in Section 4.2. A survey of similar depth to the ACS survey but over a significant area of the cluster would be required to establish the significance of this effect.

Beyond the Local Supercluster the deepest study of dwarf galaxies is of the Centaurus Cluster (45 Mpc), an

Abell (1958) richness 0 cluster. Miesgeld et al. (2009) use VLT images to study the properties of dwarf galaxies in Centaurus and determine the LF. The uncertainties from counting statistics and incompleteness are large, but the LF they find has the same general shape as Coma and Virgo: a gradual rise to about  $M_R = -13$  mag and a shallow slope fainter than this. The only Abell richness 3 clusters within 100 Mpc are Coma and Perseus (74 Mpc). The deepest measurement of the Perseus LF comes from Keck spectroscopy (Penny & Conselice 2008). The uncertainties are large but their LF is consistent with Coma as well. More distant richer clusters can only be compared with Coma at the bright end.

## 5 DISCUSSION

Based on the observations in this study, the population of galaxies in the Coma Cluster can be characterized as:

1. Most luminous galaxies in the cluster are early-type galaxies with high central surface brightnesses.
2. Most low-luminosity galaxies in the cluster are dwarf elliptical galaxies with low central surface brightnesses. Many of these are nucleated.
3. The LF has average slope  $\alpha \sim -1.5$  for  $M_I < -13$  mag. It is significantly shallower than the CDM halo mass function.
4. The LF is shallow, almost flat, at the extreme faint-end of our survey  $-13 \text{ mag} < M_I < -11$  mag. However, these measurements are less secure due to possible incompleteness.

A similar shape LF to Coma has been found in a number of environments with small crossing times and high early-type fractions e.g. the Virgo Cluster core. These are characterized by a high DGR in the range 5 – 7. Diffuse spiral-rich environments like the Ursa Major Cluster and the Local Group have a shallower LF and a smaller DGR (2 – 4).

Due to the proximity of the Coma Cluster, it can be studied in greater detail than other rich clusters. If it is typical of rich clusters, observations of Coma could strongly constrain current models of galaxy formation. Considering the observations listed above, we deduce that galaxy formation and evolution in places where there are very many galaxies tends to lead to the formation of early-type, not late-type galaxies. A number of physical processes are at work. There were probably many interactions in such environments early on when the galaxies were forming leading to formation of ellipticals. In addition, stripping by the intergalactic medium removes cold gas from galaxies on short timescales, turning off subsequent star formation activity. Whatever causes dwarf ellipticals to form in such large numbers in clusters must operate at a lower level in low-density environments. There are many possible explanations. One possible explanation is that dark-matter halos that assembled at late times (the ones in low-density environments) were not able to collect gas from the intergalactic medium (IGM) that could be turned into stars (Thoul & Weinberg 1996, Tully et al. 2002) because the IGM had been heated by previous generations of stars. Only dark-matter halos that assembled early on could become dwarf galaxies. A second explanation is that there was increased tidal activity in regions that were assembling to become clusters so that gas within dark-matter halos had a greater probability of turning into stars if the halo was in such a region. A third explanation would be that pressure confinement (Babul & Rees

1992) from hot intergalactic gas was much stronger in regions that were to become cluster cores. Another possibility would be that dwarf galaxy formation is similar in all environments, but what causes the difference in DGR between the evolved and unevolved structures is that the evolved structures are deficient in intermediate-luminosity galaxies, perhaps losing these galaxies as the central cluster galaxy builds up (Tully 2011).

Recent observations, using the same data as that described here, have discovered a population of UCDs at the core of the Coma Cluster (Madrid et al. 2010, Chiboucas et al. 2011). Such compact stellar systems had first been discovered in the Fornax Cluster in a comprehensive spectroscopic survey (Drinkwater et al. 1999, Phillipps et al. 2001, Mieske, Hilker & Infante 2002). A population of UCDs has since been discovered in the Virgo cluster (Jones et al. 2006) so UCDs may be common in evolved environments. The origin of these stellar systems is unknown and has been a subject of considerable debate. One possibility is that they are the remnants of merging star clusters and that they would be found where ever there are large numbers of globular clusters (Fellhauer & Kroupa 2002). Alternatively, it is possible that these are stripped dwarf elliptical nuclei, resulting from galaxy thrashing in clusters (Bekki et al. 2003). These galaxies could contain considerable amounts of dark matter, which would also explain the high mass-to-light ratios recently measured in such systems (Baumgardt & Mieske 2008). In this latter case, they represent systems that were genuine galaxies in the early Universe. Therefore the LF needs to be corrected for their contribution when being used to constrain galaxy formation models.

## 6 CONCLUSIONS

We have measured the LF of a 230 square arcminute region in the centre of the Coma Cluster. Brighter than  $M_I = -17$  mag, the LF agrees well with previous determinations. Between the exponential drop at bright magnitudes and  $M_I = -13$  mag, the LF is rising with average logarithmic slope  $\alpha \sim -1.5$ . Such a rise is not seen in low-density environments where the LF is slowly rising with  $\alpha \sim -1.1$  over the same magnitude range. This LF cannot continue fainter than  $M_I = -13$  mag or the number of faint members would be overprotected, but we cannot measure  $\alpha$  precisely here because of possible incompleteness and uncertainty in membership assignments at the very faint end. The LF is always much shallower than the CDM mass function. Most of the faint galaxies are dwarf ellipticals and these are preferentially found in the cluster core.

## ACKNOWLEDGMENTS

Based on observations with the NASA/ESA *Hubble Space Telescope* obtained at the Space Telescope Science Institute, which is operated by the association of Universities for Research in Astronomy, Inc., under NASA contract NAS 5-26555. These observations are associated with program GO10861. support for this work was provided in part through grant GO10561.01-96A. This research has made use of the NASA/IPAC Extragalactic Database (NED) which is

operated by the Jet Propulsion Laboratory, Caltech, under agreement with the National Aeronautics and Space Association.

## REFERENCES

- Abell G. O., 1958, *ApJS*, 3, 211  
 Adami C., Ulmer M. P., Durret F., Nichol R. C., Mazure A., Holden B. P., Romer A. K., Savine C., 2000, *A&A*, 353, 930  
 Adami C., Biviano A., Durret F., Mazure A., 2005, *A&A*, 443, 17  
 Adami C. et al., 2006, *A&A*, 459, 679  
 Adami C., Durret F., Mazure A., Pelló R., Picat J. P., West M., Meneux B., 2007a, *A&A*, 462, 411  
 Adami C., Picat J. P., Durret F., Mazure A., Pelló R., West M., 2007b, *A&A*, 472, 749  
 Adami C., Ilbert O., Pello R., Cuillandre J. C., Durret F., Mazure A., Picat J.P., Ulmer M. P., 2008, *A&A*, 491, 681  
 Adami C. et al., 2009, *A&A*, 507, 1225  
 Andreon S., Cuillandre J.-C., 2002, *ApJ*, 569, 144  
 Babul A., Rees M. J., 1992, *MNRAS*, 255, 346  
 Baumgardt H., Mieske S., 2008, *MNRAS*, in press  
 Beijersbergen M., Hoekstra H., van Dokkum P. G., van der Hulst T., 2002, *MNRAS*, 329, 385  
 Bekki K., Couch W. J., Drinkwater M. J., Shioya Y., 2003, *MNRAS*, 344, 399  
 Bernstein G. M., Nichol R. C., Tyson J. A., Ulmer M. P., Wittman D., 1995, *AJ*, 110, 1507  
 Bertin E., Arnouts S., 1996, *A&A*, 117, 393  
 Blanton M. R., Roweis S., 2007, *AJ*, 133, 734  
 Carter D. et al., 2008, *ApJS*, 176, 424  
 Chanan G. A., Abramopolous F., 1984, *ApJ*, 287, 89  
 Chiboucas K., Tully R. B., Marzke R. O., Trentham N., Ferguson H. C., Hammer D., Carter D., Khosroshahi H., 2010, *ApJ*, 723, 251  
 Chiboucas K. et al., 2011, *ApJ*, 737, 86  
 Chiboucas K., Jacobs B. A., Tully R. B., Karachentsev I. D., 2013, *AJ*, 146, 126  
 Colless M., Dunn A. M., 1996, *ApJ*, 458, 435  
 Cooray A., 2006, *MNRAS*, 356, 842  
 Drinkwater M. J., Phillipps S., Gregg M. D., Parker Q. A., Smith R. M., Davies J. I., Jones J. B., Sadler E. M., 1999, *ApJ*, 511, L97  
 Driver S. P., Couch W. J., Phillipps S., 1998, *MNRAS*, 301, 369  
 Driver S. P., Couch W. J., Phillipps S., Smith R., 1998, *MNRAS*, 301, 357  
 Fabricant D. et al., 2005, *PASP*, 117, 1411  
 Fellhauer M., Kroupa P., 2002, *MNRAS*, 330, 642  
 Ferguson H. C., Sandage A., 1988, *AJ*, 96, 1520  
 Fukugita M., Shimasaku K., Ikeuchi T., 1995, *PASP*, 107, 945  
 Fukugita M., Peebles P. J. E., 2004, *ApJ*, 616, 643  
 Godwin J. G., Peach J. V., 1977, *MNRAS*, 181, 323  
 Godwin J. G., Metcalfe N., Peach J. V., 1983, *MNRAS*, 202, 113  
 Graham A. W., Jerjen H., Guzman R., 2003, *AJ*, 126, 1787  
 Gutierrez C. M., Trujillo I., Aguerri J. A. L., Graham A. W., Caon N., 2004, *ApJ*, 602, 664  
 Hammer D. et al., 2010, *ApJS*, 191, 143  
 Hoessel J. G., Schneider D. P., 1985, *AJ*, 90, 1648  
 Jones J. B. et al., 2006, *AJ*, 131, 312  
 Karachentsev I. D., Karachentseva V. E., Richter G. M., Vennik J. A., 1995, *A&A*, 296, 643  
 Karachentsev I. D., Nasonova O. G., Courtois H. M., 2013, *MNRAS*, 429, 2264  
 Klypin A., Kravtsov A. V., Valenzuela O., Prada F., 1999, *ApJ*, 522, 82  
 Kurtz M. J., Mink D. J., 1998, *PASP*, 110, 934  
 Lieder S., Lisker T., Hilker M., Misgeld I., Durrell P., 2012, *A&A*, 538, 69

- Lisker T., 2008, ApJS, in press
- Lobo C., Biviano A., Durret F., Gerbal D., Le Fevre O., Mazure A., Slezak E., 1997, A&A, 317, 385
- Madrid J. P et al., 2010, ApJ, 722, 1707
- Mahdavi A., Trentham N., Tully R. B., 2005, AJ, 130, 1502
- Metcalfe N., Shanks T., Campos A., McCracken H. J., Fong R., 2001, MNRAS, 323, 795
- Michard R., Andreon S., 2008, A&A, 490, 923
- Mieske S., Hilker M., Infante L., 2002, A&A, 383, 823
- Mieske S., Hilker M., Infante L., Mendes de Olivera C., 2007, A&A, 463, 503
- Milne M. L., Pritchett C. J., Poole G. B., Gwyn D. J., Kovelaars J. J., Harris W. E., Hanes D. A., 2007, AJ, 133, 177
- Misgeld I., Hilker M., Infante S., 2009, A&A, 496, 683
- Mobasher B. et al., 2001, ApJS, 137, 279
- Mobasher B. et al., 2003, ApJ, 587, 605
- Mobasher B., Trentham N., 1998, MNRAS, 293, 315
- Moore B., Ghigna S., Governato F., Lake G., Quinn T., Stadel J., Tozzi P., 1999, ApJ, 524, 19
- Neumann D. M. et al., 2001, A&A, 365, L74
- Peng E. W. et al., 2009, ApJ, in press
- Penny S. J., Conselice C. J., 2008, MNRAS, 383, 247
- Phillipps S., Driver S. P., Couch W. J., Smith R. M., 1998, ApJ, 498, L119
- Phillipps S., Drinkwater M. J., Gregg M. D., Jones J. B., 2001, ApJ, 560, 201
- Price J. et al., 2009, MNRAS, 397, 1816
- Postman M., Lauer T. R., 1995, ApJ, 440, 28
- Rines K., Geller M. J., 2008, AJ, 135, 1837
- Rood H. J., Baum W. A., 1967, AJ, 72, 398
- Sabatini S., Davies J., Scaramella R., Smith R., Baes M., Linder S., Roberts S., Testa V., 2003, MNRAS, 341, 981
- Sandage A., Binggeli B., Tammann G. A., 1990, AJ, 90, 1759
- Schechter P., 1976, ApJ, 203, 297
- Schlegel D. J., Finbeiner D. P., Davis M., 1998, ApJ, 500, 525
- Schombert J. M., 1988, ApJ, 328, 475
- Secker J., 1996, ApJ, 469, L81
- Secker J., Harris W. E., 1996, ApJ, 469, 623
- Thompson L. A., Gregory S. A., 1993, AJ, 106, 2197
- Thoul A. A., Weinberg D. H., 1996, ApJ, 465, 608
- Trentham N., 1998, MNRAS, 293, 71
- Trentham N., Hodgkin S., 2002, MNRAS, 333, 423
- Trentham N., Mobasher B., 1998, MNRAS, 293, 53
- Trentham N., Sampson L., Banerji M., 2005, MNRAS, 357, 783
- Trentham N., Tully R. B., 2002, MNRAS, 335, 712
- Trentham N., Tully R. B., 2009, MNRAS, 398, 722
- Trentham N., Tully R. B., Mahdavi A., 2006, MNRAS, 369, 1375
- Trentham N., Tully R. B., Verheijen M. A. W., 2001, MNRAS, 325, 385
- Tully R. B., 2011, in EAS Publication Series Volume 48, p281
- Tully R. B., Somerville R. S., Trentham N., Verheijen M.A.W., 2002, ApJ, 569, 573
- Tully R. B., Trentham, 2008, AJ, 135, 1488
- van den Bergh S., 2000, PASP, 112, 529
- Weinmann S. M., Lisker T., Guo Q., Meyer H. T., Janz J., 2011, MNRAS, 416, 1197
- Weinzirl T. et al., 2014, MNRAS, submitted
- Yamanoi H. et al., 2012, AJ, 144, 40
- Yang X., Mo H. J., van den Bosch F. C., 2008, ApJ, 676, 248